Oregon State University

Mathematical and Computational Considerations of a Model of Microbiologically Induced Calcite Precipitation

Author
Zachary T. Barry

Advisor
Dr. Malgorzata Peszynska

An expository paper

submitted to

Oregon State University

in partial fulfillment of
the requirements for the
degree of

Master of Science

Presented May 31, 2018
Commencement June 2018

Abstract

In this paper, we discuss two possible modifications to a numerical solution method for a model of microbiologically induced calcite precipitation (MICP). MICP provides a means to seal cracks in the surfaces of geological structures. From a mathematical and computational point of view MICP has very interesting features which make it challenging for numerical solution methods to solve the system.

First, there are multiple sensitivities to every element of the system, and computational approximations to the solutions to any part of the system can effect the solution of this part very strongly. Second, a subset of the chemical reactions occur much faster than the remainder of the system. A solution method must use a fine discretization parameter to capture these dynamics, while the system must be solved on a large time scale in order for the calcite precipitation to occur. The third challenge with MICP is that some reaction terms are discontinuous, thus traditional numerical error bounds may not apply.

In this paper, we discuss two possible modifications to a numerical solution method for a model of microbiologically induced calcite precipitation (MICP). MICP provides a means to seal cracks in the surfaces of geological structures. This process can be useful in the context of carbon sequestration where even minor fissures in the storage medium can compromise the isolation of the gas.

From a mathematical and computational point of view MICP has very interesting features which make it challenging for numerical solution methods to solve the system. First, MICP models are very complex. There are multiple sensitivities to every element of the system, and computational approximations to the solutions to any part of the system can effect the solution of this part either very strongly, or not at all. Additionally, the effects can propagate to different parts of the system.

Second, a subset of the chemical reactions occur much faster than the remainder of the system. A solution method must use a fine discretization parameter to capture these dynamics, while the system must be solved on a large time scale in order for the calcite precipitation to occur. An assumption that has been used to mitigate this problem is that the reactions occur fast enough that the ratio of products to reactants remains constant. Our proposed modification is to combine the fast reactions with physical conservation laws, posing them as a system of differential algebraic equations.

The third challenge with MICP is that some reaction terms are discontinuous, thus traditional numerical error bounds may not apply. We propose to allow the precipitation rate to increase sharply on a neighborhood of the threshold instead of jumping from “off” to “on.”

Acknowledgements

First and foremost I thank my advisor, Dr. Malgorzata Peszynska, for teaching me the virtues of hard work and for providing timely and meaningful guidance.

This work was partially supported by NSF-DMS 1522734 “phase transitions in porous media across multiple scales.”

Finally, I extend my gratitude to my parents and brother for the constant love and support they have gifted me.

Contents

1 Introduction **1**

2 Mathematical and Computational Tools **3**
2.1 Useful finite differences . . . 3
2.1.1 Advection . . . 4
2.1.2 Diffusion . . . 5
2.1.3 Accuracy, stability, and convergence . . . 5
2.2 Roots of nonlinear equations . . . 7
2.3 Fractional step method . . . 8
2.3.1 Applying to multiple reactions . . . 9
2.4 Stiff systems . . . 10

3 Regularization of a discontinuous two-point BVP **11**
3.1 Weak solution . . . 11
3.2 Numerical results . . . 12

4 Calcite precipitation model **15**
4.1 Phase-field models for biofilm . . . 15
4.2 Modeling chemical reactions . . . 16
4.2.1 Four chemical models . . . 16
4.2.2 Reaction rate equations . . . 17
4.3 Numerical solution of MICP model . . . 18
4.3.1 Slow reactions . . . 19
4.3.2 Equilibrium, or "fast" reactions . . . 20
4.4 Solving the entire system . . . 22

5 Equilibrium assumption and an alternative **24**
5.1 DAEs and the calcite precipitation model . . . 24
5.2 DAE method applied to a representative subsystem. . . . 25
5.3 Comparing ODE and DAE solutions of Robertson's problem . . . 28

6 Regularizing the discontinuous precipitation term **32**
6.1 Well-posedness in reactive transport . . . 32
6.2 Yosida approximations . . . 33
6.2.1 Constructing Yosida approximations . . . 33
6.2.2 Sign graph . . . 33
6.2.3 Application to ODEs . . . 34
6.3 Applying Yosida approximations to the calcite reaction . . . 35

7 Coupled Advection-Diffusion-Reaction System **37**
7.1 Isolated initial conditions . . . 38
7.2 Results without using conservation laws . . . 39

8 Conclusions **41**

Chapter 1: Introduction

The topic of this paper is the mathematical modeling of chemical reactions. In particular, we focus on a particular model important in applications. Microbiologically induced calcite precipitation (MICP) provides a means to seal cracks in the surfaces of geological structures. This process can be useful in the context of carbon sequestration where even minor fissures in the storage medium can compromise the isolation of the gas. Figure 1.1 below contains an illustration of the orientation of the microbes, calcite, and cracks.

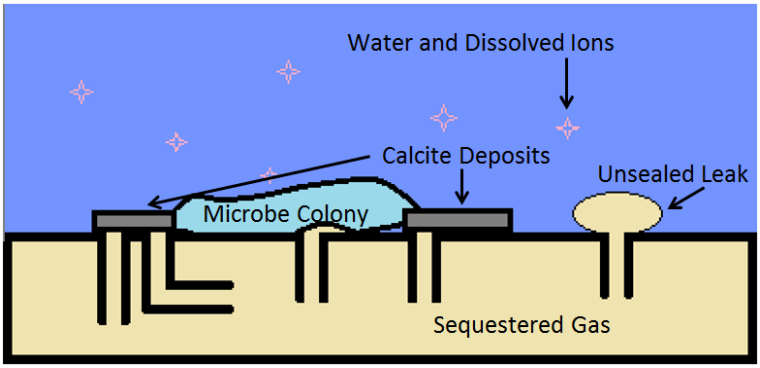

Figure 1.1: Leaks in a container filled with a sequestered gas are filled by a microbe colony which uses dissolved ions to form a calcite precipitate. Adapted from ideas in [6].

Since molecules interact in space and time on a variety of scales and under a variety of constraints, there are a variety of different ways in which one could describe the evolution of a chemical system. For a system containing N chemical species S_i, $1 \leq i \leq N$, we will consider a system of ordinary differential equations

$$\frac{\mathrm{d}S_i}{\mathrm{d}t} = r_i(S_1, \ldots, S_N), \qquad 1 \leq i \leq N. \tag{1.1}$$

To determine the reaction terms $r_1(S_1, \ldots, S_N)$, which are frequently nonlinear, we will use the mass action assumption that "the rate of any elementary reaction is always proportional to the concentration of each reactant" [9]. With this as our starting point, we will discuss two possible modifications to the numerical solution method for the MICP model presented in [17]. These modifications make it easier to solve the system numerically.

The first modification is motivated by results from numerical experiments using the original solution method. The method assumes that a subset of reactions in the calcite model occur fast enough that the ratio of products to reactants remains constant. In Section 4.3.2, we isolate one of these "fast reactions" and find that the constant ratio assumption is not satisfied. The proposed modification is to combine the fast reactions with physical conservation laws, posing them as a system of differential algebraic equations (DAEs). This is explored in Chapter 5.

The second modification seeks to smooth a discontinuous reaction term so that traditional numerical error bounds will apply. Calcium and carbonate ions only precipitate together to form calcite if their concentrations exceed a threshold value. We propose to allow the precipitation rate to increase sharply on a neighborhood of the threshold instead of jumping from "off" to "on." The regularization that we apply can be interpreted as the application of Yosida approximations to the Heaviside operator. Numerical results and a brief background on Yosida approximations are included in Chapter 6.

In real field scale applications models of MICP should include advection and diffusion in addition to reaction in the model (1.1):

$$\frac{\partial S_i}{\partial t} + a\frac{\partial S_i}{\partial x} - d\frac{\partial^2 S_i}{\partial x^2} = r_i(S). \tag{1.2}$$

The system (1.2) includes several different transport and reaction mechanisms, represented by the action of several different operators. The numerical solution to (1.2) can be split into distinct steps, one for each differential operator. Since the reaction is a zero'th order operator, the numerical solution is split into three different steps. We will apply this so called "fractional step method" to system with three reactants, and briefly explore the effect that different advection and diffusion coefficients have on the solution in Chapter 7.

The outline of this work is as follows. We will begin by recalling some computational math tools in the form of finite difference methods and iterative root finding methods in Chapter 2. In preparation for the application of these tools, we complete a preparatory problem in Chapter 3: local truncation error analysis applied to a discontinuous two point boundary value problem. In Chapter 4, we provide background on the modeling of chemical reactions and use the concepts therein to describe the calcite precipitation model. The formulation of fast chemical reactions as DAEs is compared to the equilibrium assumption of [17] in Chapter 5. We will also compare ODE and DAE solutions to Robertson's problem, a famous stiff chemical system which is introduced in [1]. Attempts to regularize the discontinuous reaction term are included in Chapter 6. Finally, in Chapter 7 we apply the finite difference techniques from Chapter 2 to an advection-diffusion-reaction system with reaction terms taken from Chapter 5.

Chapter 2: Mathematical and Computational Tools

It is rarely feasible to analytically solve a system of differential equations such as (1.2) which arise from a physical model. Therefore, we resort to numerical methods. A large class of numerical methods for approximation of solutions to PDEs is called finite difference methods.

The process of replacing differential operators with finite difference approximations results in a "large but finite algebraic system of equations" that can be solved using a mathematical programming language [10]. After going over a simple example in Section 2.1, we present sample finite differences for advection and diffusion problems. In Section 2.2 we describe how a one-sided finite difference can be used alongside Newton's method to approximate the solution to a nonlinear reaction. This is in preparation for Section 2.3 where we describe the so-called "fractional step method" and its use in solving advection-diffusion-reaction problems. We describe the difficulties associated with solving "stiff" systems of ODEs in Section 2.4.

2.1 Useful finite differences

Suppose we wanted to solve the initial value problem

$$u'(t) = f(u(t), t), \quad t \in [0, T], \qquad u(0) = u_0. \tag{2.1}$$

In case an exact solution u is hard to determine analytically, we could apply a finite difference method to obtain an approximate solution U on a finite grid of times: $U(t_n) \approx u(t_0 + nk)$.

One of the simplest algorithms is as follows:

1. Set $N \in \mathbb{N}$, $k = \frac{T}{N}$. Partition $[0, T]$ by the grid points $\{nk\}_{n=0}^{N} = \{t_n\}_{n=0}^{N}$.
2. Set $U(0) = u_0$ and require that $U(t_n) = U_n$ satisfy

$$\frac{U_n - U_{n-1}}{k} = f(U_n, t_n), \quad j = 1, \ldots, J. \tag{2.2}$$

   Then the grid values are given as

$$U_n = kf(t_n) + U_{n-1}, \quad n = 1, \ldots, N. \tag{2.3}$$

3. If the exact solution $u(x)$ is known, calculate $u(t_n)$, $1 \leq n \leq N$. Consider the grid values and exact values as $N \times 1$ column vectors $\overline{U}$ and $\overline{u}$, respectively. Use a prescribed norm $\|\cdot\|$ to evaluate the size of the global error $\overline{U} - \overline{u}$.

The finite difference approximation (2.3) is known as explicit Euler, and the grid solutions converge to $u(x)$ as $N \to \infty$.

For the purposes of this section, we will assume our problems are posed for $x \in [0, 1]$ and $t \in [0, T]$ for some $T > 0$. The time discretization is given by $\{nk\}_{n=0}^{N}$, $Nk = 1$. In space, we have $\{jh\}_{j=0}^{J}$, $Jh = 1$. Let U_j^n represent the grid solution at $(x, t) = (jh, nk)$. U^n will be used to describe the solution at time $t = nk$, $\{U_j^n\}_{j=0}^{J}$. Similarly define U_j.

2.1.1 Advection

In general, an advection initial value problem takes the form

$$\begin{cases} au_x + u_t = 0, & 0 < x < C,\ 0 < t,\ 0 < a; \\ u(0,t) = f(t), & 0 \le t; \\ u(x,0) = g(x), & 0 \le x \le C. \end{cases} \tag{2.4}$$

We will begin by discussing where initial and boundary conditions should be prescribed, as well as the compatibility conditions they must satisfy in order that $u \in C^1$. We will then present a simple finite difference scheme for the numerical solution of the problem.

Where to prescribe initial and boundary conditions. Notice that

$$(a, 1) \cdot (u_x, u_t) = 0,$$

implying that solutions are constant along lines parallel to $(a, 1)$. The line that contains an arbitrary point (x_0, t_0) and is parallel to $(a, 1)$ is given by

$$t - t_0 = \frac{1}{a}(x - x_0). \tag{2.5}$$

The intersection of (2.5) with the x-axis occurs when $x = x_0 - at_0$. Thus, if $x_0 - at_0 > 0$, our initial condition informs us that $u(x_0, t_0) = u(x_0 - at_0, 0) = g(x_0 - at_0)$. However, if $x_0 - at_0 < 0$, we are out of the domain of our initial condition. We now look to the boundary condition to inform our solution, concluding that

$$u(x,t) = \begin{cases} g(x - at), & \text{if } x > at, \\ f(t - a^{-1}x), & \text{if } x < at. \end{cases} \tag{2.6}$$

Suppose we change the PDE to $-au_x + u_t = 0$. Then the same discussion leads us to the solution

$$u(x,t) = \begin{cases} g(x + at), & \text{if } x > -at, \\ f(t + a^{-1}x), & \text{if } x < -at. \end{cases}$$

Since the problem is posed on the first quadrant, it is always the case that $x > -at$. So $u(x,t) = g(x + at)$ and thus $u(0,t) = g(at)$. But our boundary condition requires $u(0,t) = f(t)$. In general, $g(at) \neq f(t)$; the problem is not well-posed. The problem would become well posed if instead of specifying $u(0,t) = f(t)$, $0 \le t$, we specified $u(C,t) = f(t)$, $0 \le t$.

For the half space advection problem data can be posed on any initial curve $\gamma \colon \mathbb{R}^+ \to \mathbb{R}^2$, $\gamma(s) = (x_0(s), t_0(s))$, for which $(a, 1)$ is "not parallel to the tangent $(x_0'(s_0), t_0'(s_0))$ [of γ]" [12]. That is, γ must satisfy

$$\begin{vmatrix} x_0'(s_0) & t_0'(s_0) \\ a & 1 \end{vmatrix} = (a, 1) \cdot (-t_0'(s_0), x_0'(s_0)) \neq 0$$

for all $s_0 \ge 0$. Such a curve is referred to as being "non-characteristic."

Guaranteeing a C^1 solution. We recall from [2] that the solution $u(x,t)$ to (2.4) is C^1 if the initial and boundary conditions are C^1 and satisfy the "compatibility relations"

$$f(0) = g(0), \qquad ag'(0) + f'(0) = 0. \tag{2.7}$$

That is, the data must agree at the origin and the PDE must be satisfied at the origin. Otherwise, the solution (2.6) only satisfies the PDE away from the line $x = at$.

Numerical Solution Methods. Assume the grid solution U^n is known. We will use explicit Euler (2.3) to approximate u_t and a similar one sided approximations to u_x. There are two options for approximating u_x, though:

$$(a) \quad u_x(jh,\cdot) = \frac{U_{j+1} - U_j}{h} + \tau_j, \qquad (b) \quad u_x(jh,\cdot) = \frac{U_j - U_{j-1}}{h} + \tau_j. \tag{2.8}$$

Here, τ_j is the local truncation error (LTE) of the approximation (discussed below). As presented in [10], these approximations lead to two different numerical methods for solving (2.4):

$$(a) \quad U_j^{n+1} = U_j^n - \frac{ak}{h}(U_j^n - U_{j-1}^n), \qquad (b) \quad U_j^{n+1} = U_j^n - \frac{ak}{h}(U_{j+1}^n - U_j^n). \tag{2.9}$$

Do we use the information to the left of U_j^n (as in (2.9a)) or the information to the right (as in (2.9b)) to find U_j^{n+1}?

Recall from our discussion about the data for the quarter plane problem that if $a > 0$, the boundary condition should be supplied on the left side. Thus if $a > 0$ (as in (2.4)) then (2.9a) is the correct method to use; (2.9a) is sometimes referred to as an "upwind" method. Notice that (2.9a) only determines $\{U_j^{n+1}\}_{j=1}^J$; the solution for U_0^{n+1} relies on the nonexistent point U_{-1}^n. The left boundary condition completes the grid solution: first set $U_0^{n+1} = f((n+1)k)$, then use (2.9a) J times to solve for $\{U_j^{n+1}\}_{j=1}^J$. Note that the upwind method is only stable if $0 \le \frac{ak}{h} \le 1$.

2.1.2 Diffusion

Two boundary conditions are used when posing a diffusion problem. We will consider the case when constant in time Dirichlet conditions β and γ are specified at $x = 0$ and $x = 1$, respectively. Fixing a final time T, our diffusion problem is to find $u(x,t)$ such that

$$\begin{cases} u_t - du_{xx} = 0, & 0 < x < 1,\ 0 < t \le T; \\ u(0,t) = \beta, & 0 < t; \\ u(1,t) = \gamma, & 0 < t; \\ u(x,0) = h(x), & 0 \le x \le 1. \end{cases} \tag{2.10}$$

We will use the *centered difference approximation* to u_{xx}:

$$u_{xx}(jh,(n+1)k) = \frac{U_{j-1}^{n+1} - 2U_j^{n+1} + U_{j+1}^{n+1}}{h^2} + \tau_j. \tag{2.11}$$

Combining (2.11) with a one sided finite difference approximation for u_t, we see that

$$U_j^{n+1} - \frac{k}{h^2}(U_{j-1}^{n+1} - 2U_j^{n+1} + U_{j+1}^{n+1}) = U_j^n \tag{2.12}$$

for interior nodes. A linear system of equations arises from (2.12), in which we satisfy the boundary conditions as in Section 2.1.1.

2.1.3 Accuracy, stability, and convergence

If we apply a finite difference method to a differential equation, we would like to know whether or not the global error decays to zero as the number of grid points grows. That is, we would like to know if the method is *convergent*. Before discussing convergence, we will state the definition of local truncation error.

Local Truncation Error. The error which results from approximating a derivative by a finite difference method is called the local truncation error (LTE). To calculate the LTE, the grid values in a finite difference method are replaced with the exact solution at those points. Next, Taylor expansions are taken about the current grid value and the coefficients on the terms $u^{(q)}$ are collected where $1 \leq q \leq Q$ and Q is the number of derivatives taken in the Taylor expansions. The leading term that remains after terms are collected is of the form $Ch^p u^{(l)}(x_j)$ where C is a constant, h is the step size, and x_j is the grid point about which the expansions are taken. Then if τ_j is the LTE at x_j, $\tau_j = \mathcal{O}(h^p)$ as $h \to 0$.

The solution is sometimes required to be smoother than the order of the LTE. For example, the centered difference approximation (2.11) has LTE that behaves like $\mathcal{O}(h^2)$ as the grid is refined. However, the first five terms of the solution's Taylor series are required to prove this estimate so the solution must be known to be at least $C^4([0,1] \times [0,T])$ (in the case of Equation (2.10)). In Chapter 6 we will apply the centered difference approximation to a problem where the solution is discontinuous, obtaining a different order for the LTE.

Convergence. Suppose $U = [U^0, U^1, \ldots, U^N]$ is a regular grid approximation of the solution to an ODE on the interval $[0,T]$; $N = T/k$. Let $u = [u(0), u(k), \ldots, u(Nk)]^T$ represent the exact solution restricted to the grid. Then the global error is $E^k = U - u$. The method used to obtain U is convergent provided $\lim_{k \to 0} \|E^k\| = 0$ where $\|\cdot\|$ is a prescribed vector norm. We recall the q grid function norm $\|\cdot\|_{\Delta,q}$ as defined in [10]. If E is a vector containing difference between the exact and numerical solution at each point of a regular discretization with N grid points, then

$$\|E\|_{\Delta,q} = \left(h \sum_{i=1}^{N} |E_i|^q \right)^{1/q}.$$

In Chapter 3, we will recall that the solution error from applying the centered difference approximation can be bounded above by the LTE times a constant. We will consider the problem $u''(x) = f(x)$ where $f(x)$ is discontinuous and determine the theoretical order of the LTE when $f(x)$ is replaced by a regularized right hand side $f_\epsilon(x)$.

Calculating the order of convergence. Suppose that the error associated with a numerical scheme behaves like $\|E(h)\|_{\Delta,q} \approx Ch^p$, where $E(h)$ is the error when the spatial discretization parameter h is used. We would like to approximate the order of convergence p by comparing results from a finite set spatial discretization parameters.

Suppose we have error vectors E_m, $1 \leq m \leq 4$, arising from discretization parameters h_m, where $h_m > h_n$ for $m < n$. Recall that if $\|E_m\|_{\Delta,q} = C_m h_m^{p_m}$, then

$$\ln(\|E_m\|_{\Delta,q}) = \ln(C_m) + p_m \ln(h_m). \tag{2.13}$$

So we have three pairs of equations with two unknowns, C_m and p_m, of the form

$$\begin{bmatrix} \ln(\|E_{m-1}\|_{\Delta,q}) \\ \ln(\|E_m\|_{\Delta,q}) \end{bmatrix} = \begin{bmatrix} 1 & \ln(h_{m-1}) \\ 1 & \ln(h_m) \end{bmatrix} \begin{bmatrix} \ln(C_m) \\ p_m \end{bmatrix}. \tag{2.14}$$

With solutions given by

$$\frac{1}{\ln(h_m) - \ln(h_{m-1})} \begin{bmatrix} \ln(h_m) & \ln(-h_{m-1}) \\ -1 & 1 \end{bmatrix} \begin{bmatrix} \ln(\|E_{m-1}\|_{\Delta,q}) \\ \ln(\|E_m\|_{\Delta,q}) \end{bmatrix} = \begin{bmatrix} \ln(C_m) \\ p_m \end{bmatrix}. \tag{2.15}$$

We can use (2.15) to find three estimates of the true p value, p_2, p_3, and p_4. These gives use the averaged estimate,

$$p \approx \frac{\sum_{m=2}^{4} p_m}{3}. \tag{2.16}$$

Frequently, the ratio $\frac{h_m}{h_{m+1}}$ is chosen to be constant.

2.2 Roots of nonlinear equations

Fix a point x in the spatial domain and consider the problem

$$u_t(x,t) = f(u(x,t)), \tag{2.17}$$

where $u_t(x,t) = \frac{\partial u(x,t)}{\partial t}$. Obviously, if f is linear in u then the problem is easily solved. Chemical reactions, however, are frequently nonlinear, such as in (1.1). Now we approximate the solution to (2.17) numerically, using the finite difference approach introduced above. First, approximate the time derivative in (2.17):

$$\frac{U^{n+1} - U^n}{k} - f(U^{n+1}) = 0. \tag{2.18}$$

Now we see that (2.18) is nonlinear, and may not be amenable to provide a closed form solution. Instead we seek a solution by iteration.

We rewrite (2.18) equivalently as follows.

$$F(U^{n+1}) = U^{n+1} - U^n - kf(U^{n+1}) = 0. \tag{2.19}$$

We seek to solve (2.19) by Newton iteration. We note that in practice we solve (2.19) at every point x_j of spatial grid, i.e., for every j. Thus the spatial subscript U_j is omitted for brevity as the following discussion applies anywhere in space. In practice, Newton's method seeks U^{n+1} so that the magnitude of $F(U^{n+1})$ is smaller than a tolerance value ϵ.

We will make three assumptions: a root U^{n+1} exists, F' is Lipschitz continuous on the domain of interest, and $F'(U^{n+1}) \neq 0$. These three assumptions are called "standard assumptions" in [7]. And as proved in Theorem 5.1.2 in [7], these three assumptions are sufficient conditions for Newton's method to converge q-quadratically to U^{n+1} from any initial guess within some distance δ of U^{n+1}. Note that in the context of reaction rate equations, the reaction terms are polynomial. While it may be challenging to find the Lipschitz constant, we are guaranteed that the function is locally Lipschitz. Since the method should converge rapidly if the existence and Lipschitz conditions are satisfied, we implement a stringent stopping procedure: if the method fails to converge after ≈ 5 steps, we refine k and restart.

Newton's method starts with an initial guess of the value of U^{n+1}, labeled $U^{r,0}$. For the purposes of this discussion, $U^{r,0} = U^n$; if the behavior of F were well understood a different initial guess could be selected. Notice that if $|F(U^{r,0})| < \epsilon$, the guess is accepted and we have a stationary solution. Supposing the first i guesses fail to satisfy the tolerance condition, $U^{r,i+1}$ would be calculated as the solution to

$$0 = F(U^{r,i}) + F'(U^{r,i})(U^{r,i+1} - U^{r,i}). \tag{2.20}$$

Equivalently,

$$U^{r,i+1} = U^{r,i} - (F'(U^{r,i}))^{-1} F(U^{r,i}). \tag{2.21}$$

Assuming the initial guess was in $V \cap (U^{n+1} - \delta, U^{n+1} + \delta)$, we know that F' is nonsingular and that convergence is guaranteed.

2.3 Fractional step method

Let $u(x,t) = [u_1(x,t), \ldots, u_m(x,t)]^T$ represent the concentrations of m chemical species at the point $x \in \mathbb{R}$ at time t, and consider the advection-diffusion-reaction equation,

$$u_t + au_x - du_{xx} = r(u). \tag{2.22}$$

Boundary conditions and an initial solution profile are prescribed depending on the application.

Rather than solving the entire partial differential equation at once, we take an approach suggested by [10]. This approach is called a fractional step method, and it works by splitting up the equation into three pieces, advancing each piece separately in time. A benefit of this method is that it "allows us to use very different methods for each piece" of the PDE (2.22). Let $\mathcal{S}_1$ represent a numerical advection scheme, $\mathcal{S}_2$ a numerical scheme for a first-order in time ODE, and $\mathcal{S}_3$ a numerical diffusion scheme. Suppose we have a grid solution U^n at time $t = nk$. We can split (2.22) up and solve for U^{n+1} as follows:

$$U^* = \mathcal{S}_1(U^n, k) \tag{2.23}$$

$$U^{**} = \mathcal{S}_2(U^*, k) \tag{2.24}$$

$$U^{n+1} = \mathcal{S}_3(U^{**}, k). \tag{2.25}$$

However, this approach is likely only first-order accurate. Note that there are higher order splitting methods, but we will not consider these here.

To see this, we extend [10]'s example (pg. 238) of a linear system of ODEs with two constant coefficient matrices to an example with three matrices to accommodate the fact that we are using three numerical methods to solve (2.22). Consider

$$u_t = Au + Bu + Cu \tag{2.26}$$

where $A, B, C \in \mathbb{R}^{m \times m}$. Since this problem is linear, the exact solution is given by $u(t) = e^{(A+B+C)t}u(0)$.

Supposing we start on some grid point $t_n = nk$ and advance the exact solution to t_{n+1}. We have that the true solution

$$u(t_{n+1}) = e^{(A+B+C)(t_n+k)}u(0) = e^{(A+B+C)k}e^{(A+B+C)t_n}u(0) = e^{(A+B+C)k}u(t_n). \tag{2.27}$$

Alternatively, suppose we solve for the solution at time t_{n+1} via the fractional step method. That is, starting at the (exact) grid solution U^n, we find

$$U^{n+1} = e^{Ck}U^{**} = e^{Ck}e^{Bk}U^* = e^{Ck}e^{Bk}e^{Ak}U^n. \tag{2.28}$$

Consider the difference $U^{n+1} - u(t_{n+1})$ between the exact solution to (2.27) and that given by (2.28). Replacing the matrix exponentials with their Taylor series representations, we have

$$\begin{aligned} U^{n+1} - u(t_{n+1}) = (I + kC + \frac{1}{2}k^2C^2 + \cdots)(I + kB + \frac{1}{2}k^2B^2 + \cdots)(I + kA + \frac{1}{2}k^2A^2 + \cdots) \\ - (I + k(A+B+C) + \frac{1}{2}k^2(A+B+C)^2 + \cdots). \end{aligned}$$

Notice that while the first order terms cancel, the quadratic terms will only cancel if the matrices A, B, and C, commute. However, matrices are not commutative in general so the one step error $|U^{n+1} - u(t_{n+1})|$ has a magnitude of $O(k^2)$. Therefore the fractional step method is only first order accurate; there is no benefit to be gained by using higher order methods for the intermediate steps.

2.3.1 Applying to multiple reactions

Consider a system of coupled advection-diffusion-reaction problems

$$\begin{aligned}(u_1)_t + a(u_1)_x - d(u_1)_{xx} &= -K_1 u_1,\\ (u_2)_t + a(u_2)_x - d(u_2)_{xx} &= K_1 u_1 - K_2 u_2,\\ (u_3)_t + a(u_3)_x - d(u_3)_{xx} &= K_2 u_2.\end{aligned} \tag{2.29}$$

The process of solving the system (2.29) will be split up by a fractional method as described above. That is, we will assume the species are not coupled through advection or diffusion. We will begin by solving the intermediate advection problem for each species. Then we use a reaction solver to solve the coupled reaction terms before solving the intermediate diffusion problem for each species.

The need for the decoupled assumption. Suppose u_1, u_2, and u_3 *were* coupled through advection and diffusion. Let $U_l^{n,j}$ be the grid solution for species l at the point (nk, jh), and assume that $a > 0$. Then, using the upwind and centered finite differences for advection and diffusion, respectively, our problem would be to simultaneously solve

$$\frac{U_l^{n+1,j} - U_l^{n,j}}{k} + a\frac{U_l^{n+1,j} - U_l^{n+1,j-1}}{h} - d\frac{U_l^{n+1,j-1} - 2U_l^{n+1,j} + U_l^{n+1,j+1}}{h^2} = f_l(U_1^{n+1,j}, U_2^{n+1,j}, U_3^{n+1,j}), \quad 1 \le l \le 3$$

for each interior grid value U_l^{n+1}, $1 \le l \le 3$. Clearly, this is much more computationally demanding then assuming that only the reaction term is coupled between the species. We proceed to describe the process of solving the coupled reaction term below.

Newton's Method for a coupled reaction system.

Fix a point x in the spatial domain and let $f_i(u_1, u_2, u_3)$, $i = 1, 2, 3$, represent the three reactions in (2.29). Then we can use implicit Euler to approximate $(u_i)_t$ so that the intermediate reaction problems become

$$\frac{U_l^{n+1} - U_l^n}{k} = f_l(U_1^{n+1}, U_2^{n+1}, U_3^{n+1}), \quad l = 1, 2, 3. \tag{2.30}$$

As before, the spatial subscript U_j is omitted; the index l is used to keep track of the solution component. We rearrange (2.30) so that we are solving for a zero of an equation:

$$F_l(U_1^{n+1}, U_2^{n+1}, U_3^{n+1}) = U_l^{n+1} - U_l^n - k f_l(U_1^{n+1}, U_2^{n+1}, U_3^{n+1}) = 0. \tag{2.31}$$

Given the previous concentration vector $U^n = [U_1^n, U_2^n, U_3^n]^T$, and an initial guess $U^{r,0} = [U_1^{r,0}, U_2^{r,0}, U_3^{r,0}]$ for the post-reaction concentrations which solve (2.31), we can use Newton's method to improve the guess. This guess is improved until a concentration vector is found so that $F(U^{r,i}) = [F_1(U^{r,i}), F_2(U^{r,i}), F_3(U^{r,i})]^T$ satisfies $\|F(U^{r,i})\| < \epsilon$ for a prescribed norm $\|\cdot\|$ and tolerance ϵ.

Recall that in Section 2.2, we applied Newton's method in just one step. For the coupled system, we include an intermediate step as in Algorithm 5.3.1 in [7]. Let $S^{r,i} = [S_1^{r,i}, S_2^{r,i}, S_3^{r,i}]^T$ represent a correction term that we add to our current guess $U^{r,i}$ in order to improve it. That is, suppose $U^{r,i+1} = U^{r,i} + S^{r,i}$. Then $F'(U^{r,i})S^{r,i} = -F(U^{r,i})$ where $F'(U^{r,i})$ is the Jacobian matrix of F evaluated at $U^{r,i}$. To solve for $S^{r,i}$, one could use a linear solver such as Matlab's backslash \ command.

2.4 Stiff systems

Now we consider the difficulties associated with solving the reaction step as in (2.29). For the sake of exposition we consider only linear reaction terms. Then in the case of a system with m chemical species $u_i(t)$, $1 \leq i \leq m$, our problem is of the form $u'(t) = Au(t)$ where $A \in \mathbb{R}^{m \times m}$ consists of reaction rate constants and $u(t) = [u_1(t), \ldots, u_m(t)]^T$.

Suppose A is diagonalizable with eigenvalues λ_i and corresponding eigenvectors v_i, $1 \leq i \leq m$. It is a standard result that $u_i(t) = e^{\lambda_i t} v_i$, $1 \leq i \leq m$, are solutions to $u'(t) = Au(t)$. Then

$$u(t) = \sum_{i=1}^{m} c_i e^{\lambda_i t} v_i, \qquad c_i \in \mathbb{R},\ 1 \leq i \leq m$$

is the general solution of the system. Since the v_i are linearly independent, c_i can be selected to satisfy any initial condition.

It may be challenging for finite difference methods to provide an accurate approximation of the solution if the ratio between the magnitudes of the eigenvalues is large. This is due to the fact that the time discretization k for the numerical solution must be small in order to capture the fast moving dynamics (associated with large $|\text{Re } \lambda_i|$). However, the system must be solved until a large final time T in order to capture the slow moving dynamics (associated with small $|\text{Re } \lambda_i|$). As the "stiffness ratio"

$$\frac{\max_{i=1,2,\ldots,n} |\text{Re } \lambda_i|}{\min_{i=1,2,\ldots,n} |\text{Re } \lambda_i|}$$

increases, so does the number of grid values $N = T/k$ required for the stability of explicit finite differences.

One could avoid this problem by using an A-stable finite difference. The reason for this is that "if an A-stable [method] is applied to a stiff system....no stability restriction on [k] can result" [8]. However, there are no explicit A-stable methods, and those implicit methods which are A-stable can be no more than second order [8]. Additionally, implicit methods are often more computationally demanding than explicit methods. As we will see in Section 4.3.2, some researchers have approached this difficulty by solving the differential equations which evolve rapidly separately from those which evolve relatively slowly.

Chapter 3: Regularization of a discontinuous two-point BVP

In this chapter, we discuss numerical solution of a "rough" second order boundary value problem (BVP) which has a discontinuous right hand side f.

Consider the following two-point BVP:

$$-u''(x) = f = \begin{cases} 0 & \text{if } x < 0.5 \\ 1 & \text{if } x \geq 0.5, \end{cases} \qquad \begin{cases} u(0) = 0 \\ u(1) = 0, \end{cases} \tag{3.1}$$

where $x \in (0,1)$. Since f has a jump discontinuity, there is no classical solution to this problem.

In what follows we first discuss the framework in which (3.1) has a solution, called a "weak solution". A classical solution can be found if instead we consider a smoother problem in which f is replaced by a smooth function f_ϵ. Then we demonstrate that the traditional analysis of error via truncation error analysis combined with stability does not demonstrate superiority of the regularization in the finite difference approximation.

3.1 Weak solution

Let $u, v \in H_0^1((0,1))$ to obtain the variational or weak formulation of the problem:

$$a(u,v) = \int_0^1 u'(x)v'(x)\mathrm{d}x = \int_0^1 f(x)v(x)\mathrm{d}x. \tag{3.2}$$

The theory guarantees the existence of a solution $u \in H_0^1((0,1))$ to (3.1) [12]. If $a(u,v)$ is strongly elliptic then since $f \in L^2((0,1))$, any $u \in H_0^1((0,1))$ which satisfies (3.2) will also satisfy $u \in H_0^2((0,1))$ [13].

We recall the definition of strong ellipticity for operators on intervals I in $\mathbb{R}$ [13]: let a_0, a_1, $a_{11} \in L^\infty(I)$. Then the sesquilinear form

$$a(u,v) = \int_I \left(a_{11}(x)u'(x)v'(x) + a_0(x)u(x)v(x) + a_1(x)u'(x)v(x)\right)\mathrm{d}x, \qquad u, v \in H^1(I) \tag{3.3}$$

is strongly elliptic if there exists $c > 0$ such that

$$a_{11}(x)a^2 \geq c|a|^2, \qquad a \in \mathbb{R}, \quad x \in I. \tag{3.4}$$

Notice that for our problem $a_{11} = 1$ and $a_0 = a_1 = 0$; $a(u,v)$ is trivially strongly elliptic on the interval $(0,1)$ with $c = 1$.

We recall the Sobolev embedding theorem which tells us that $H^m((0,1)) \subset C_u^k$ whenever $m > k + \frac{n}{2}$ in the sense that every function in $H^m((0,1))$ is equal almost everywhere equal to a uniquely determined function in $C_u^k((0,1))$ [13]. Here, C_u^k refers to the set of uniformly continuous functions whose partial derivatives are all uniformly continuous up to (and including) order k. Since the the inequality holds for

$(m = 1, k = 0)$ and $(m = 2, k = 1)$, u is identified with a continuously differentiable function on $(0, 1)$.

This is enough information to determine an analytical solution to the problem. Integrating the differential equation twice gives us

$$u(x) = \begin{cases} c_1 x + c_2, & \text{if } x < 0.5, \\ \frac{1}{2}x^2 + c_3 x + c_4, & \text{if } x \geq 0.5. \end{cases}$$

Requiring that $u(x)$ vanishes on the boundary and that $u(x)$ and $u'(x)$ are continuous identifies the constants of integration:

$$u(x) = \begin{cases} \frac{1}{8}x & \text{if } x < 0.5, \\ -\frac{1}{2}x^2 + \frac{5}{8}x - \frac{1}{8} & \text{if } x \geq 0.5. \end{cases} \tag{3.5}$$

Linear regularization. We modify Equation 3.1 to linearly increase from $u''_\epsilon(x) = 0$ to $u''_\epsilon(x) = 1$ on an ϵ-neighborhood about $x = 0.5$. One could apply a higher order regularization, but this complicates the process of determining the constants of integration for the exact solution. Consider the modified problem

$$f_\epsilon = -u''_\epsilon(x) = \begin{cases} 0, & \text{if } x < 0.5 - \epsilon \\ \dfrac{x - (0.5 - \epsilon)}{2\epsilon}, & \text{if } x \in [0.5 - \epsilon, 0.5 + \epsilon] \\ 1, & \text{if } x > 0.5 + \epsilon \end{cases}, \quad \begin{cases} u(0) = 0 \\ u(1) = 0 \end{cases}. \tag{3.6}$$

Since f_ϵ is continuous, a classical analytical solution to (3.6) can be found by imposing the same continuity requirements as on $u(x)$. It is important to note that the analytical solution to (3.6) is independent of ϵ when $x \notin (0.5 - \epsilon, 0.5 + \epsilon)$.

3.2 Numerical results

We will be using the centered difference method (2.11) to solve (3.1) and (3.6). Let U_h represent the numerical solution to (3.1) using spatial width h. Let $U_{h,\epsilon}$ represent the numerical solution to (3.6) using spatial width h, and regularization width ϵ. Table 3.1 below reports $\|U_h - U_{h,\epsilon}\|_{\Delta,2}$ for various (h, ϵ) pairings. Table 3.2 reports the associated convergence rates for fixed h and decreasing ϵ (i.e. row-wise p values).

		Regularization ϵ^{-1}				
		10	100	1,000	10,000	100,000
Spatial h^{-1}	10	7.2887×10^{-3}	7.2887×10^{-3}	7.2887×10^{-3}	7.2887×10^{-3}	7.2887×10^{-3}
	100	8.3808×10^{-4}	7.2176×10^{-4}	7.2176×10^{-4}	7.2176×10^{-4}	7.2176×10^{-4}
	1,000	4.3570×10^{-4}	7.2323×10^{-5}	7.2169×10^{-5}	7.2169×10^{-5}	7.2169×10^{-5}
	10,000	4.2978×10^{-4}	8.6449×10^{-6}	7.2170×10^{-6}	7.2169×10^{-6}	7.2169×10^{-6}

Table 3.1: $\|U_h - U_{h,\epsilon}\|_{\Delta,2}$ where h is fixed along each row and ϵ is fixed along each column.

Observe that in Table 3.1, the error stays nearly constant along each row for $\epsilon \leq h/10$. This results in the zeros we see in Table 3.2 along each row for $\epsilon \leq h$. This is due to the fact that when 2ϵ becomes smaller than h, numerical solutions

		Regularization ϵ^{-1}				
		10	100	1,000	10,000	100,000
Spatial h^{-1}	10	N/A	0	0	0	0
	100	N/A	0.064894	0	0	0
	1,000	N/A	0.7799	9.234×10^{-4}	0	0
	10,000	N/A	1.6965	0.07840	9.4387×10^{-6}	0

Table 3.2: The ratios $[\ln(\|U_h - U_{h,1\times10^{-m}}\|_{\Delta,2} - \ln(\|U_h - U_{h,1\times10^{-m+1}}\|_{\Delta,2})]/[\ln(1\times10^{-m}) - \ln(1\times10^{-m+1})]$, $2 \le m \le 5$, which approximate the order of convergence as ϵ is refined as discussed in Equation (2.15).

to (3.6) are no longer sampling in the domain of regularization. And since $f_\epsilon(x)$ is independent of ϵ for $x \notin (0.5-\epsilon, 0.5+\epsilon)$, $f_{\epsilon'}(x) = f_\epsilon(x)$ for all $\epsilon < \frac{h}{2},\ \epsilon' < \frac{h}{2}$.

For $h < \frac{1}{10{,}000}$, the resulting numerical grid was too fine for MATLAB to process the code. Therefore, we do not have enough data points to determine the order of convergence of $u_{h,\epsilon}$ to u_h for any ϵ. Based on the above discussion, our conclusion is that if an ϵ regularization (3.6) is applied to (3.1), solving the system for $h > 2\epsilon$ will result in the same amount of error, $\sqrt{h}\|u_h - u_{h,\epsilon}\|_2$, as would $h = 2\epsilon$.

Bounding solution error. For a given discretization, let A be the matrix that presents the centered difference method as $AU = F$ where F is a vector containing the values of f at the grid points and U is a vector containing the grid solution. Let $\tilde{U}$ be the true solution to (3.1) at the grid points so that $A\tilde{U} = F + \tau$, where τ is the LTE. Then $E = U - \tilde{U}$ is a vector of the solution error at each grid point. Notice $AE = -\tau$, the local truncation error at each grid point. Recall that A is non-singular for any value of h, so we can express $E = -A^{-1}\tau$. Taking the vector 2-norm of each side,

$$\|E\|_2 \le \|A^{-1}\|_2 \cdot \|\tau\|_2. \tag{3.7}$$

Note that the size of A depends on how small h is. The centered difference method is said to be *stable* if $\|A^{-1}\|_2$ is bounded independent of h for h sufficiently small. Indeed, it can be shown that $\|A^{-1}\|_2 \approx \frac{1}{\pi^2}$ for small h.

Recall that $\|E\|_{\Delta,q} = h^{1/q}\|E\|_q$. Thus, if (3.7) holds, then

$$\|E\|_{\Delta,2} = \sqrt{h}\|E\|_2 \le \sqrt{h}\|A^{-1}\|_2\|\tau\|_2 = \|A^{-1}\|_2\|\tau\|_{\Delta,2}. \tag{3.8}$$

Obviously, E and τ can be replaced by E^ϵ and τ^ϵ. We proceed to calculate $\|\tau\|_{\Delta,2}$ and $\|\tau^\epsilon\|_{\Delta,2}$ in order to obtain a bound on $\|E\|_{\Delta,2}$ and $\|E^\epsilon\|_{\Delta,2}$.

The LTE at a point x_j can be found by substituting the exact solution u_j into the FDM, and subtracting the second-order derivative $f(x_j)$ from it:

$$\tau_j = \frac{1}{h^2}(-u(x_{j-1}) + 2u(x_j) - u(x_{j+1})) - f(x_j). \tag{3.9}$$

We would like to use Taylor series expansions of $u(x_{j-1})$ and $u(x_{j+1})$ about x_j, but u is not even twice differentiable on the entire interval $[0,1]$, in spite of being smooth on $(0,1/2)$ and $(1/2,1)$.

First, we proceed with formal Taylor expansions. Using the Lagrange form of the remainder for a Taylor polynomial,

$$u(x_{j-1}) = u(x_j) - hu'(x_j) + \frac{h^2}{2}u''(\xi_-), \quad \xi^- \in (x_{j-1}, x_j), \tag{3.10}$$

$$u(x_{j+1}) = u(x_j) + hu'(x_j) + \frac{h^2}{2}u''(\xi^+), \quad \xi^+ \in (x_j, x_{j+1}). \tag{3.11}$$

Substitute (3.10) and (3.11) into (3.9), and replace $f(x_j)$ with $-u''(x_j)$, to obtain

$$\tau_j = -\frac{1}{2}(u''(\xi) + u''(\xi')) + u''(x_j). \tag{3.12}$$

Now we take into account the singularity of the derivatives of u near $1/2$. In fact we see that a nonzero LTE can be observed at most twice: when $x_j < 0.5 < x_{j+1}$, τ_j and τ_{j+1} can both be $-\frac{1}{2}$.

Let $\tau = [\tau_1, \ldots, \tau_m]^{\mathrm{T}}$. Then

$$\|\tau\|_{\Delta,2} \leq \frac{\sqrt{2}}{2}\sqrt{h}. \tag{3.13}$$

Inequality (3.13) suggests that we can express $\|E\|_{\Delta,2} = \mathcal{O}(h)$.

We can now repeat the analysis for the regularized problem, restricting our attention to the case $\epsilon < 0.25$. This restriction makes sense because our goal in regularizing the discontinuous BVP is to enhance its numerical convergence while retaining its original structure as much as possible.

Let $M = \frac{2\epsilon}{h} + 2$, the maximum number of grid points that can reside within a distance h of the region where regularization takes place. Taylor expansions of the solution u_ϵ to the regularized problem about x_j (with the Lagrange remainder) and observations about $f_\epsilon(x)$ tell us that

$$\|\tau^\epsilon\|_{\Delta,2} \leq \sqrt{h} \cdot \sqrt{\sum_{k=1}^{M+2} |\frac{1}{2}|^2} \leq \sqrt{h}\left(\sqrt{\frac{\epsilon}{2h}} + \frac{\sqrt{2}}{2}\right) = \frac{\sqrt{2}}{2}(\sqrt{\epsilon} + \sqrt{h}). \tag{3.14}$$

Notice that as ϵ approaches 0, the bound on $\|\tau^\epsilon\|_2$ approaches that of $\|\tau\|_2$.

We recall from our stability discussion above that $\|A^{-1}\|_2 \approx \frac{1}{\pi^2}$ for small h, to conclude from (3.7) that

$$\|E\|_{\Delta,2} \leq \frac{\sqrt{2}}{2\pi^2}\sqrt{h}, \qquad \|E^\epsilon\|_{\Delta,2} \leq \frac{\sqrt{2}}{2\pi^2}\left(\sqrt{\epsilon} + \sqrt{h}\right). \tag{3.15}$$

Thus, the centered difference method applied to the discontinuous problem is $\mathcal{O}(h^{1/2})$; applied to the regularized problem the method is $\mathcal{O}(\epsilon^{1/2} + h^{1/2})$. We conclude that linearly regularizing the problem offers no clear improvement to the numerical results. However, it is possible that applying a quadratic or other higher order regularization would improve the numerical results.

Chapter 4: Calcite precipitation model

In this chapter we will consider a model of biofilm induced calcite precipitation and its numerical solution. We will begin by summarizing the work in [15] and [16] which describe the ability of this model to predict the growth of biofilm colonies in Section 4.1. With this larger context in mind, in Section 4.2 we provide the background on modeling chemical reactions necessary for our description of the entire model in Section 4.3. This description will include the numerical procedure that [17] uses to solve it. We will conclude by identifying two components of the numerical procedure that could be replaced by alternatives. These alternatives are investigated in Chapters 5 and 6.

4.1 Phase-field models for biofilm

The situation [15] seeks to model is a follows: bacteria feeds on a nutrient present in a solvent and builds communities by producing extracellular polymeric substance (EPS), a group of molecules which hold the bacteria together. The authors consider several phase-field models for biofilms and use numerical experiments to determine which model best represents the expected behavior of the system. They treat the system as one fluid which consists of two components: (a) bacteria and EPS; (b) nutrient and solvent. This setup benefits the authors since they avoid the potentially complicated interface conditions that arise when treating the system as two separate fluids.

The authors notice that the polymer volume fraction and nutrient substrate will each be transported at a different speed due to relative force of their mixing. This leads them to using the Cahn-Hilliard equation (CHE) (with a reaction term for polymer production) to describe the transport. In the case of the polymer, the CHE describes the phase separation between itself and the biofilm as mixing occurs. They also obtain the modified Cahn-Hilliard (MCHE) equation by assuming a proportionality constant is itself proportional to the polymer volume fraction. It is the difference between these formulations that the authors focus on in their numerical experiments.

For the numerical experiments the authors assume the average velocity will be zero relative to the solid boundary (no-slip condition) and prescribe a no-flux boundary condition on the volume fraction of the polymer network. They assume a constant level of nutrient is being fed through the top boundary. Their results show that the biofilm in the EPS network is transported to regions with less polymer. As the mobility constant increases, this transport becomes faster. The merit of the MCHE over the CHE becomes clear when the volume fraction of the polymer is allowed to grow. Since the MCHE depends on the polymer volume fraction while the CHE does not, the MCHE model responds well when the polymer vanishes while the CHE model is susceptible to numerical error.

In [16], the authors use their findings from [15] to run numerical experiments on a 2-D grid. They focus on applying the model to a cavity and shear cell. The boundary conditions which characterize the cavity are given by vanishing normal

fluxes for the nutrient flow, polymeric flow, and polymer network volume fraction. The average velocity of the fluid on the boundary is also set to vanish. The shear cell is characterized by the same conditions in the transverse direction and by periodic conditions in the direction of flow. In both cases, a "feeding condition" is allowed to introduce nutrients through the top of the domain.

They first run the cavity case with a nonzero feeding condition applied to an initial polymer configuration that is uniform except for a hump in the middle. The result is that the hump expands outwards in all directions, and it corroborates the usefulness of the model. It is noted that the expansion of the polymer is primarily a result of the mixing discussed in [15].

Weak and strong shears (slow and fast boundary velocities at the top of the cell) are compared against different EPS production levels and bacteria configurations. The authors find that if the interface between the biofilm and the solvent is rough, then the colonies are more likely to detach. A smooth interface causes a small layer of biofilm to detach, leaving the structure of the base relatively unchanged. Strong shear flow magnifies these findings. Finally, higher EPS production is found to have a profound effect on the structural stability of the colonies. In the case of strong sheer, initial colony configurations that we would expect to detach in the absence of EPS production are able to weather the stress without detaching (although significant deformation occurs).

4.2 Modeling chemical reactions

This section is based on several fundamental references from applied mathematics and geochemistry. First, we follow [3] to discuss four modeling options ranging from the chemical master equation (which generally requires too much computational power to be practical) to the reaction rate equation (which we will be using throughout this paper) in Section 4.2.1. We set up the notation for reaction rate equations in Section 4.2.2. Note that the different types of models are also associated with different time scales. The most practical and observable time scale is associate with the reaction rate equations on which we eventually focus.

4.2.1 Four chemical models

First we will give a brief overview of the different equations that can be used to describe chemical dynamics. All equations are formed under the assumption that the chemical dynamics are the same throughout the spatial domain. That is, they are formed under the assumption that the system is "well stirred."

The most computationally demanding equation, the Chemical Master Equation (CME) is a system of ordinary differential equations (ODEs). There is one ODE for each possible state of the system. To grasp the size of this equation, consider the simple forward reaction $A \to B$. Let $X(t) = [N(A)(t),\ N(B)(t)]^T$ represent the state of the system where $N(A)(t)$ and $N(B)(t)$ are the number of molecules of A and B at time t, respectively. Suppose $X(0) = [N,\ 0]^T$. Then the collection of all possible future states can be listed as

$$\begin{bmatrix} N \\ 0 \end{bmatrix}, \begin{bmatrix} N-1 \\ 1 \end{bmatrix}, \begin{bmatrix} N-2 \\ 2 \end{bmatrix}, \ \cdots, \ \begin{bmatrix} 1 \\ N-1 \end{bmatrix}, \begin{bmatrix} 0 \\ N \end{bmatrix}.$$

[3] refers to the above as *state vectors*. The CME for this reaction has dimension $N + 1$ because there are $N + 1$ possible state vectors. In general, if there are N

molecules to be distributed among S species there are

$$\frac{(N+S-1)!}{N!\,(S-1)!}$$

possible states of the system. If we are modeling a real world problem, N will not be small.

Instead of keeping track of each possible state of the system, we can write a stochastic differential equation for each species. That is, we use $Y(t)$ to describe the state of the system where $Y(t)$ is "a continuous time, real-valued stochastic process—at each time t, $Y_i(t)$ is a real-valued random variable representing the number of molecules of the ith species" [3]. The dimension of this system, the Chemical Langevin Equation (CLE), is now determined by the number of species. Note that $Y_i(t)$ is not necessarily a whole number as $X_i(t)$ is in the CME. Thus, there is a hidden assumption that needs to be satisfied for the CLE to be a good model: that the number of molecules of each species in the system is large.

Finally, we can transition from stochastic differential equations to ordinary ones to obtain reaction rate equations (RREs). These are explored in the next section.

4.2.2 Reaction rate equations

In this section, we will be dealing with *elementary reactions*. This is in contrast to *overall reactions*. Elementary reactions "mechanistically describe the stepwise transformations at the molecular level" while overall reactions "represent the net result of a series of elementary reactions" [9]. A classic example of an overall reaction is the Michaelis-Menten reaction. In it, a substrate is transformed into a product after an intermediate step where it bonds with an enzyme. This reaction is covered in more depth in Chapter 7.

There are three common elementary reactions which [3] calls "first order", "second order," and "dimerization" reactions:

first order	second order	dimerization
$A \to P$	$A + B \to P$	$A + A \to P.$

The RRE come from the physical property that "the rate of any elementary reaction is always proportional to the concentration of each reactant" [9]. If we let $k > 0$ be a general proportionality constant, then the rates of the reactions listed above are give as

first order	second order	dimerization
$\frac{\mathrm{d}[P]}{\mathrm{d}t} = k[A]$	$\frac{\mathrm{d}[P]}{\mathrm{d}t} = k[A][B]$	$\frac{\mathrm{d}[P]}{\mathrm{d}t} = k[A]^2$
$\frac{\mathrm{d}[A]}{\mathrm{d}t} = -k[A]$	$\frac{\mathrm{d}[A]}{\mathrm{d}t} = \frac{\mathrm{d}[B]}{\mathrm{d}t} = -k[A][B]$	$\frac{\mathrm{d}[A]}{\mathrm{d}t} = -2k[A]^2$

In this context, k is called a reaction rate constant. This idea can be extended to a reaction in which three species collide as is done in Section 4.3 below.

Note that $\mathrm{d}[A]/\mathrm{d}t = -\mathrm{d}[P]/\mathrm{d}t$ in each elementary reaction since A is being depleted at the same rate P is being created. Also note that if $P = 2C$ for some chemical species C, then the RRE for C is

$$\frac{\mathrm{d}[C]}{\mathrm{d}t} = 2\frac{\mathrm{d}[C]}{\mathrm{d}t}.$$

We do not square the concentration of C as we do for A in the dimerization reaction because we are not describing the likelihood with which a molecule of C collides with another C.

We conclude this portion of the discussion by describing the RRE of three species which are involved in two reactions:

$$2A + B \underset{k_{-1}}{\overset{k_1}{\rightleftharpoons}} C. \tag{4.1}$$

Note that (4.1) describes the following reactions simultaneously:

$$\begin{aligned} &\text{(i)} \quad 2A + B \xrightarrow{k_1} C, \\ &\text{(ii)} \quad C \xrightarrow{k^{-1}} 2A + B. \end{aligned} \tag{4.2}$$

The RREs for (4.2)(i) are

$$\frac{\mathrm{d}[C]}{\mathrm{d}t} = k_1[A]^2[B] = -\frac{\mathrm{d}[B]}{\mathrm{d}t}, \quad -2k_1[A]^2[B] = \frac{\mathrm{d}[A]}{\mathrm{d}t}.$$

The RREs for (4.2)(ii) are

$$2\frac{\mathrm{d}[A]}{\mathrm{d}t} = \frac{\mathrm{d}[B]}{\mathrm{d}t} = k^{-1}[C] = -\frac{\mathrm{d}[C]}{\mathrm{d}t}.$$

To find the RREs for (4.1), we merely sum the contributions from (4.2)(i) and (4.2)(ii):

$$\begin{aligned} \frac{\mathrm{d}[A]}{\mathrm{d}t} &= -k_1[A]^2[B] + \tfrac{1}{2}k^{-1}[C], \\ \frac{\mathrm{d}[B]}{\mathrm{d}t} &= -k_1[A]^2[B] + k^{-1}[C], \\ \frac{\mathrm{d}[C]}{\mathrm{d}t} &= k_1[A]^2[B] - k^{-1}[C]. \end{aligned}$$

This method of determining the RREs of a system of chemical reactions will be used below in Section 4.3 and later on in Chapter 7.

4.3 Numerical solution of MICP model

The chemical species included in the calcite precipitation model are listed below in Table 4.1.

Table 4.1: The letters S and F indicate if a species participates in a slow reaction, a fast reaction, or both. The scientific name of each species is listed beneath its molecular formula.

$1S$ $[CO(NH_2)_2]$ Urea	$2SF$ $[NH_3]$ Ammonia	$3SF$ $[H_2CO_3]$ Carbonic Acid	$4F$ $[NH_4^+]$ Ammonium
$5F$ $[OH^-]$ Hydroxide	$6F$ $[HCO_3^-]$ Bicarbonate	$7SF$ $[CO_3^{2-}]$ Carbonate	$8S$ $[Ca^{2+}]$ CalciumIon
$9F$ $[Cl^-]$ Chlorine Ion	$10F$ $[H^+]$ Hydrogen Ion	$11S$ $[CaCO_3]$ Calcium Carbonate	

Before setting up the RREs of each species, we consider the "governing equation" from [17]:

$$\frac{\partial S_i}{\partial t} + \nabla \cdot (S_i \mathbf{v}) = \nabla \cdot (D_i \nabla S_i + a z_i S_i \nabla \zeta) + R_i \tag{4.3}$$

Let each species be associated with the number i given in Table 4.1. Then S_i represents the concentration of species i, D_i is its diffusion coefficient, R_i is its slow chemical reaction term (0 if the species does not participate in a slow reaction), a is a constant, and ζ is the electric potential. We ignore the transport terms in order to simplify the equation. This leaves us with

$$\frac{dS_i}{dt} = R_i \tag{4.4}$$

for each of the eleven species, $1 \leq i \leq 11$.

The eleven species are split into two groups, those which participate in slow reactions and those which participate in fast reactions. [17] asserts that fast chemical reactions "occur rapidly relative to diffusion...and can thus be assumed to be at quasi-equilibrium." That is, the fast reactions do not contribute terms the RREs of the involved species. Since the species S_i, $i = 4, 5, 6, 9, 10$, are only involved in fast reactions, $R_i = 0$ for $i = 4, 5, 6, 9, 10$. However, these species do not have fixed concentrations; instead of describing their dynamics with reaction rate equations, [17] describes them as having a constant ratio of products to reactants. We will refer to this as the "equilibrium method," giving more details in Section 4.3.2.

4.3.1 Slow reactions

First, we focus our attention on the two slow reactions:

$$\mathrm{CO(NH_2)_2 + 2H_2O \rightarrow 2NH_3 + H_2CO_3} \tag{4.5}$$

$$\mathrm{CO_3^{2-} + Ca^{2+} \rightarrow CaCO_3} \tag{4.6}$$

Reaction (4.5) is "urea hydrolysis," wherein urea breaks down in water. The reaction rate constant is given by k_u. Reaction (4.6) is "calcite precipitation," where $\mathrm{CO_3^{2-}}$ and $\mathrm{Ca^{2+}}$ combine to form solid $\mathrm{CaCO_3}$. Notice that neither reaction is reversible. From (4.5), obtain the following RREs:

$$\frac{\mathrm{d[CO(NH_2)_2]}}{\mathrm{d}t} = -k_u[\mathrm{CO(NH_2)_2}], \tag{4.7}$$

$$\frac{\mathrm{d[NH_3]}}{\mathrm{d}t} = 2k_u[\mathrm{CO(NH_2)_2}], \tag{4.8}$$

$$\frac{\mathrm{d[H_2CO_3]}}{\mathrm{d}t} = k_u[\mathrm{CO(NH_2)_2}]. \tag{4.9}$$

Note that there is no RRE for $\mathrm{H_2O}$ since it is assumed to be supplied in excess.

Reaction (4.6) only occurs if the calcite saturation stage S (defined in RRE (4.10) below), exceeds a critical value, S_{crit}. Note that S depends on a constant K_{SO}, called the equilibrium calcite solubility product. [17] list $S_{\text{crit}} = 50$, a dimensionless quantity. With this value, the RREs for the species involved in reaction (4.6) are discontinuous:

$$\frac{\mathrm{d[CO_3^{2-}]}}{\mathrm{d}t} = \frac{\mathrm{d[Ca^{2+}]}}{\mathrm{d}t} = -\frac{\mathrm{d[CaCO_3]}}{\mathrm{d}t} = \begin{cases} -k_p(S-1)^2, & S \geq S_{\text{crit}} \\ 0, & S < S_{\text{crit}} \end{cases}, \quad S = \frac{[\mathrm{Ca^{2+}}][\mathrm{CO_3^{2-}}]}{K_{SO}}. \tag{4.10}$$

The definition of $\mathrm{K_{SO}}$ is similar to that of another value, $\mathrm{K_{SP}}$, the solubility product. Every solid substance is soluble to some degree in water, and K_{SP} is the product of the concentration of dissolved ions [11]. We put forward an interpretation of $\mathrm{K_{SO}}$ as $\mathrm{K_{SP}} = [\mathrm{Ca^{2+}}_{(aq)}][\mathrm{CO_3^{2-}}_{(aq)}]$ when $\mathrm{CaCO_{3(s)}} \rightleftharpoons \mathrm{Ca^{2+}}_{(aq)} + \mathrm{CO_3^{2-}}_{(aq)}$ is at equilibrium. Recall that the numerator of S is the product of the total concentration of calcium and carbonate ions in solution (i.e. the product of the sum of dissolved calcite ions and the ions present from other reactions). Since these sums must be greater than or equal to the dissolved ions, this interpretation implies that $S \geq 1$.

4.3.2 Equilibrium, or "fast" reactions

To see how the quasi-equilibrium assumption is incorporated into the model from [17], we consider one of the fast chemical reactions that takes place as part of the calcite precipitation model:

$$\mathrm{HCO_3^-} \overset{K_2}{\longleftrightarrow} \mathrm{H^+} + \mathrm{CO_3^{2-}} \tag{4.11}$$

The rate constant K_2 in this reaction is expressed as a constant ratio of ion concentrations:

$$K_2 = \frac{[\mathrm{H^+}][\mathrm{CO_3^{2-}}]}{[\mathrm{HCO_3^-}]}. \tag{4.12}$$

The challenge is to understand how this constant is obtained in the context of forward and backward reactions. We discuss this below by considering the forward and backward reactions separately.

Interpretation of the rate constant K_2. We interpret K_2 by separating the two-way reaction (4.11) into forward and backward reactions, each with their own unique rate constant F_2 and B_2, respectively.

$$\begin{aligned} \mathrm{HCO_3} &\xrightarrow{\mathrm{F_2}} \mathrm{H^+} + \mathrm{CO_3^-} \\ \mathrm{H^+} + \mathrm{CO_3^-} &\xrightarrow{\mathrm{B_2}} \mathrm{HCO_3} \end{aligned} \tag{4.13}$$

We use (4.13) to write the RREs for the above species:

$$\frac{\mathrm{d}[\mathrm{HCO_3^-}]}{\mathrm{d}t} = -F_2[\mathrm{HCO_3^-}] + B_2[\mathrm{CO_3^{2-}}][\mathrm{H^+}] \tag{4.14}$$

$$\frac{\mathrm{d}[\mathrm{CO_3^{2-}}]}{\mathrm{d}t} = F_2[\mathrm{HCO_3^-}] - B_2[\mathrm{CO_3^{2-}}][\mathrm{H^+}] \tag{4.15}$$

$$\frac{\mathrm{d}[\mathrm{H^+}]}{\mathrm{d}t} = F_2[\mathrm{HCO_3^-}] - B_2[\mathrm{CO_3^{2-}}][\mathrm{H^+}]. \tag{4.16}$$

In quasi-equilibrium, each of the left-hand side of the ODEs (4.14)-(4.16) are assumed to be equal to zero. Therefore, in quasi-equilibrium we can separate the concentration terms from the rate terms to obtain the following ratio:

$$\frac{[\mathrm{CO_3^{2-}}][\mathrm{H^+}]}{[\mathrm{HCO_3^-}]} = \frac{F_2}{B_2}. \tag{4.17}$$

We notice that (4.17) is of the same form of (4.12), with $\frac{\mathrm{F_2}}{\mathrm{B_2}} = \mathrm{K_2}$.

Now we want to check how close are the solutions to the ODE system (4.14)-(4.16) to satisfying (4.17). In other words, we can solve the ODEs, and calculate the ratio $\frac{[\mathrm{CO_3^{2-}}][\mathrm{H^+}]}{[\mathrm{HCO_3^-}]}$ even before the steady-state solution is attained. This helps to assess the robustness of the equilibrium modeling assumptions.

To this end, we solve the system of RREs (4.14)-(4.16) for initial conditions and rate constants given as

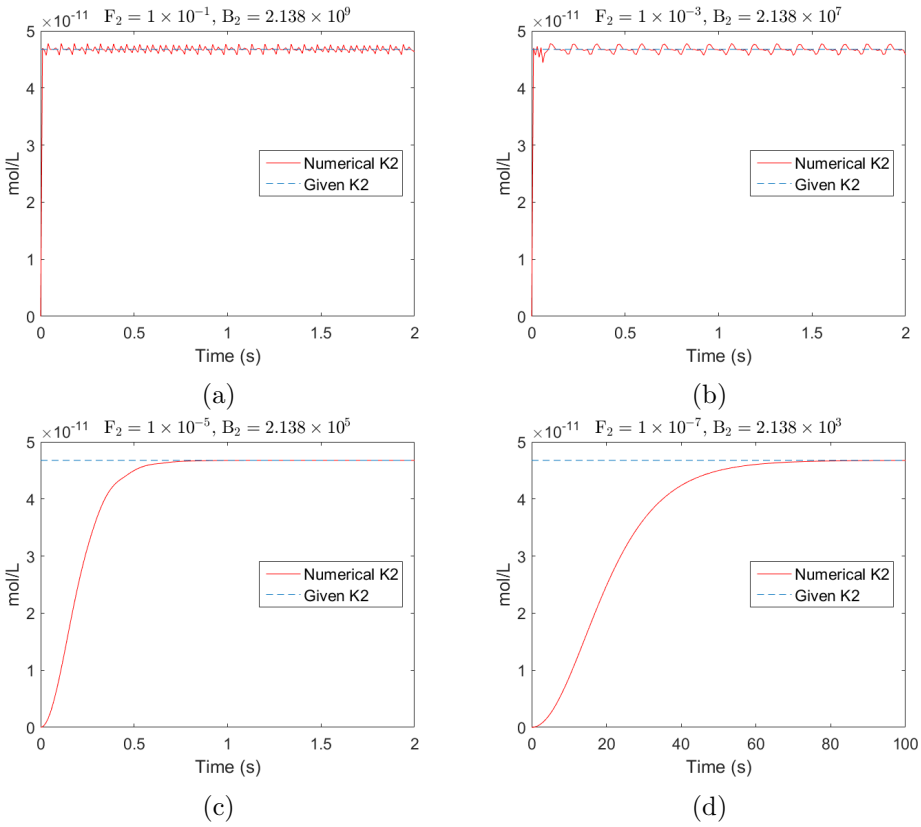

Figure 4.1: The numerical rate constant value oscillates about the value given in [17] in Figures 4.1a and 4.1b, where $F_2 = 1 \times 10^{-1}$ and $F_2 = 1 \times 10^{-3}$, respectively. For the smaller F_2 values of 1×10^{-5} and 1×10^{-7} in Figures 4.1c and 4.1d, the numerical K_2 does not agree with the given value as quickly. Once it reaches the steady-state solution, though, it is a better match than in Figures 4.1a and 4.1b.

$$S_6(0) = 10\text{mol/L},\ S_7(0) = 0\text{mol/L},\ S_{10}(0) = 0\text{mol/L},$$
$$F_2 = 1 \times 10^{-j},\ B_2 = 2.138 \times 10^{j+10},\ j = 1, 3, 5, 7$$

where $\mathrm{F_2/B_2} = 4.6774 \times 10^{-11}$mol/L, the K_2 value from [17].

The reactions with fast rates are clearly very stiff, thus would call for an implicit time integrator, which would call for a nonlinear solver such as Newton's method. As we explained in Chapter 2 the numerical solution produced would have an error due to the time discretization and another due to the nonlinear solver. Since our focus in this section is on the modeling error between equilibrium and fast reactions, we choose therefore to use a professionally written ODE solver from MATLAB, the native MATLAB ODE solver, `ode45`, so we can focus on non-numerical aspects of the problem.

The solver delivers the numerical solutions corresponding to F_2 and B_2. We plot the numerical K_2 value, $K_{2,\,\mathrm{num}}$, by plugging the concentrations obtained in the experiment into Equation (4.17). A reference line at the height of the exact value is included in Figure 4.1 below.

For the tests with the largest forward rate constants, $F_2 = 1 \times 10^{-1}$ and $F_2 = 1 \times 10^{-3}$ in Figures 4.1a and 4.1b, the numerical rate constant quickly increases to oscillate about the value given in [17] The oscillations have similar amplitudes, but the frequency is higher in Figure 4.1a. For the tests with the smaller forward rate constants, $F_2 = 1 \times 10^{-5}$ and $F_2 = 1 \times 10^{-7}$ in Figures 4.1c and 4.1d, the numerical rate constant takes a relatively long period of time to meet the given value. It takes

approximately 1 second for them to meet in Figure 4.1c and 80 seconds in Figure 4.1d. The discrepancies between the numerical results and the K_2 value from [17] encourage us to investigate an alternative solution method in Chapter 5.

4.4 Solving the entire system

We will first detail how the system is solved in [17] and then list our simplified version.

1. Initialize volume fractions of solvent, biomaterial, and calcite ($\phi_s,\ \phi_b\ \phi_c$), velocity ($\mathbf{v}$, external flow), and molecule concentrations (S_i).
2. (i) Determine the total concentration of nitrogen, N_T, and (ii) determine the total concentration of carbon, C_T, in the solution.
3. (i) Solve for the concentration of hydrogen ions and (ii) solve for the concentration of the molecules that participate in fast (equilibrium) reactions.
4. Determine the electric potential of the system, ζ.
5. Time-step the transport and momentum equations to update mass fractions and system velocity.
6. Time-step the ODE terms in the species' mass-transport equations to solve for the concentration of molecules that participate in slow reactions.
7. Move to time $t + \Delta t$ and return to step 2.

Since our focus is on the fast reactions and discontinuous precipitation ODE, we remove the steps that require solving PDEs and modify certain equations to include only ODEs. Our new procedure is as follows

(A) Initialize concentrations, S_i, and fix the volume fraction of biofilm.

(B) (i) Determine the total concentration of nitrogen, N_T, and (ii) determine the total concentration of carbon, C_T, in the solution.

(C) (i) Solve for the concentration of hydrogen ions and (ii) solve for the concentration of the molecules that participate in fast (equilibrium) reactions using ratios similar to (4.12).

(D) Time-step the ODE terms in the species' mass-transport equations to solve for the concentration of molecules that participate in slow reactions..

(E) Move to time $t + \Delta t$ and return to step 2.

Equations (4.18), (4.19), (4.20), (4.21) and (4.22) below correspond to computational steps B(i), B(ii), C(i), C(ii), and D, respectively.

$$[NH_4^+] + [NH_3] = N_T \tag{4.18}$$

$$[\mathrm{H_2CO_3}] + [\mathrm{HCO_3^-}] + [\mathrm{CO_3^{2-}}] = C_T \tag{4.19}$$

$$\frac{N_T K_3[\mathrm{H^+}]}{1 + K_3[\mathrm{H^+}]} + [\mathrm{H^+}] - \frac{K_w}{[\mathrm{H^+}]} - \frac{C_T}{\dfrac{[\mathrm{H^+}]}{K_1} + 1 + \dfrac{K_2}{[\mathrm{H^+}]}} - \frac{2C_T}{\dfrac{[\mathrm{H^+}]^2}{K_1 K_2} + \dfrac{[\mathrm{H^+}]}{K_2} + 1} = -2[\mathrm{Ca^{2+}}] + [\mathrm{Cl^-}] \tag{4.20}$$

$$[\mathrm{NH_3}] = \frac{N_T}{K_3[\mathrm{H^+}] + 1}, \quad [\mathrm{NH_4^+}] = \frac{N_T K_3[\mathrm{H^+}]}{K_3[\mathrm{H^+}] + 1}, \quad \text{(similarly for } [\mathrm{H_2CO_3}], [\mathrm{HCO_3^-}], \text{ and } [\mathrm{CO_3^{2-}}]) \tag{4.21}$$

$$\frac{dS_i}{dt} = R_i \text{ where } S_i \text{ is the concentration of species } i \tag{4.22}$$

Solving for $[H^+]$**.** Notice that in (4.20), $[Ca^{2+}]$, $[Cl^-]$, N_T, and C_T are all known from initial conditions for the first time step, and are known from (4.22) for subsequent time steps. $K_i,\ 1 \leq i \leq 3$ are constants that represent the ratio of other ions to $[H^+]$. K_w is the water disassociation constant (the degree to which H_2O dissociates into H^+ and OH^-). Thus Equation (4.20) is a nonlinear equation $f([H^+])$ which we can solve (4.20) using an iterative root finding method, such as Newton's Method as was described in Section 2.2.

Picking a time step and initial conditions. It should be noted that when implementing this solution scheme, the choice of time step seems to be an important factor. When solving the system with the same initial conditions as in [17], time steps coarser than approximately 7 seconds returned nonphysical solutions (i.e. species with negative concentrations). Further investigation of this threshold is outside of the scope of this paper.

Chapter 5: Equilibrium assumption and an alternative

In this chapter, we compare two different ways of solving a chemical system which contains reactions that occur on very different time scales. In particular, we examine the equilibrium method from Section 4.3.2 and present an alternative kinetic solution using differential algebraic equations (DAEs).

In Section 5.1 we give a short background on DAEs and describe their connection to the calcite precipitation model. Unfortunately, due to the size of the resulting system and the interdependence of the species involved, it is beyond the scope of this paper to attempt to determine how the DAE formulation for the entire MICP system effects the solutions. Instead, we compare the DAE and ODE formulations for small systems by conducting two different numerical experiments.

The first experiment is devised so that the effect on the chemistry can be observed, the second experiment attempts to compare convergence rates. These results are included in Sections 5.2 and 5.3, respectively.

5.1 DAEs and the calcite precipitation model

A system of DAEs differs from a system of ODEs in that some equations specify $y_i(t)$ and not $y_i'(t)$. In this case, $y_i(t)$ is called an *algebraic* variable. A system of ODEs can by obtained from a system of DAEs by differentiating the algebraic variables a sufficient number of times. This number is sometimes referred to as the *index* of the DAE [1]. As a simple example of the difference between the two, consider the following:

$$\text{(a)} \quad \begin{aligned} y_1'(t) &= f(t) \\ y_2'(t) &= g(t) \end{aligned}, \qquad \text{(b)} \quad \begin{aligned} y_1'(t) &= m(t) \\ y_2(t) &= n(t) \end{aligned}. \tag{5.1}$$

In this case the ODE (5.1)(a)can be obtained from the DAE (5.1)(b) by differentiating $y_2(t)$ to obtain the relationship $y_2'(t) = n'(t)$.

Sometimes some algebraic variables $y_i(t)$ are not defined explicitly, but rather implicitly. For example, if a DAE is created by combining an ODE with some constraint, it is represented as a *semi-explicit DAE*:

$$\begin{aligned} y' &= f(t, y, z) \\ 0 &= g(t, y, z) \end{aligned}, \quad (z \text{ algebraic}). \tag{5.2}$$

The fast reactions in the calcite model can be describe in the semi-explicit form.

Connection to calcite model. Let $\mathcal{S}_F$ refer to a vector containing the fast reactants. We will associate each $S_i \in \mathcal{S}_F$, $i \neq 10$, with an ordinary differential equation $f_i(t, \mathcal{S}_F)$. This is in contrast to the assumption made in [17], that $f_i(t, \mathcal{S}_F) = 0$ for each $S_i \in \mathcal{S}_F$. We will treat S_{10} as an algebraic variable, describing its behavior with a charge conservation law $g(\mathcal{S}_F)$. If $F = [f_i(t, \mathcal{S}_F)]^T$, then the semi-explicit form is

$$\begin{aligned} \mathcal{S}_F'(t) &= F(t, \mathcal{S}_F) \\ 0 &= g(t, S_F). \end{aligned}.$$

The charge constraint g ensures that the system has a neutral net charge after the fast reactions are solved. Note that the slow species $[Ca^{2+}]$ and $[Cl^-]$ are fixed during the fast reactions, their concentrations are treated as a parameter of g to be updated after each iteration of the solution. In order for the charges to balance,

$$g(t, \mathcal{S}_F) = [NH_4^+] - [OH^-] - [HCO_3^-] - 2[CO_3^{2-}] + [H^+] + [Ca^{2+}] - [Cl^-] = 0.$$

We return to our reaction rate equations to express $F(t, \mathcal{S}_F)$:

$$\begin{aligned}
[NH_3]'(t) &= f_1(t, \mathcal{S}_F) = -F_3[NH_3] + B_3[NH_4^+][OH^-] \\
[H_2CO_3]'(t) &= f_2(t, \mathcal{S}_F) = -F_1[H_2CO_3][OH^-]^2 + B_1[OH^-][HCO_3^-] \\
[NH_4^+]'(t) &= f_3(t, \mathcal{S}_F) = F_3[NH_3] - B_3[NH_4^+][OH^-] \\
[OH^-]'(t) &= f_4(t, \mathcal{S}_F) = -F_1[H_2CO_3][OH^-]^2 + B_1[OH^-][HCO_3^-] - F_2[OH^-][HCO_3^-] + \cdots \\
&\qquad \cdots + B_2[CO_3^{2-}] + F_3[NH_3] - B_3[NH_4^+][OH^-] \\
[HCO_3^-]'(t) &= f_5(t, \mathcal{S}_F) = F_1[H_2CO_3][OH^-]^2 - B_1[OH^-][HCO_3^-] - F_2[OH^-][HCO_3^-] + B_2[CO_3^{2-}] \\
[CO_3^{2-}]'(t) &= f_6(t, \mathcal{S}_F) = F_2[OH^-][HCO_3^-] - B_2[CO_3^{2-}]
\end{aligned}$$

Thus, the matrix representation of our system of differential algebraic equations is

$$\begin{bmatrix} 1 & 0 & 0 & 0 & 0 & 0 & 0 \\ 0 & 1 & 0 & 0 & 0 & 0 & 0 \\ 0 & 0 & 1 & 0 & 0 & 0 & 0 \\ 0 & 0 & 0 & 1 & 0 & 0 & 0 \\ 0 & 0 & 0 & 0 & 1 & 0 & 0 \\ 0 & 0 & 0 & 0 & 0 & 1 & 0 \\ 0 & 0 & 0 & 0 & 0 & 0 & 0 \end{bmatrix} \begin{bmatrix} [NH_3]'(t) \\ [H_2CO_3]'(t) \\ [NH_4^+]'(t) \\ [OH^-]'(t) \\ [HCO_3^-]'(t) \\ [CO_3^{2-}]'(t) \\ [H^+]'(t) \end{bmatrix} = \begin{bmatrix} f_1(t, \mathcal{S}_F) \\ f_2(t, \mathcal{S}_F) \\ f_3(t, \mathcal{S}_F) \\ f_4(t, \mathcal{S}_F) \\ f_5(t, \mathcal{S}_F) \\ f_6(t, \mathcal{S}_F) \\ g(t, \mathcal{S}_F)) \end{bmatrix}. \tag{5.3}$$

The singular left hand matrix is referred to as the *mass matrix*, and MATLAB has two solvers — `ode15s` and `ode23t` — which are capable of solving systems in this form.

To get a sense of how DAE formulation effects the chemistry, we conduct numerical tests on a smaller system which has dynamics representative of (5.3). The results and discussion are included in Section 5.2 below. We will also conduct a grid refinement analysis on the ODE and DAE approaches, using fine grid solutions in place of a true solution. This analysis is done on numerical solutions to the classic stiff chemical system called Robertson's problem using the same MATLAB solver `ode15s`. The computational costs of the methods are also compared. This is all included in Section 5.3.

5.2 DAE method applied to a representative subsystem.

Consider the variables A, B, C, and D, which can be interpreted as chemical species. The evolution of A, B, and D are governed by

$$\frac{\mathrm{d}A}{\mathrm{d}t} = -\frac{\mathrm{d}B}{\mathrm{d}t} = -\frac{\mathrm{d}D}{\mathrm{d}t} = -\gamma A + \delta BD, \qquad \frac{\mathrm{d}C}{\mathrm{d}t} = r. \tag{5.4}$$

We assume they must satisfy two conservation laws:

$$\begin{aligned}
&\text{(a)} \quad A(t) + 2B(t) - 2C(t) - D(t) = 0, \\
&\text{(b)} \quad A(t) + B(t) = A(0) + B(0).
\end{aligned} \tag{5.5}$$

These two laws could be interpreted as a charge neutrality condition and an atomic conservation condition, respectively. Notice that (5.5)(b) should always hold since $\mathrm{d}A/\mathrm{d}t + \mathrm{d}B/\mathrm{d}t = 0$.

Suppose we want to solve this system from time $t_0 = 0$ to time T with N grid points. Let $\{A_i(nk)\}_{n=0}^{N}$ be the grid solution values of A, similarly for B, C, and D. Then the equilibrium method is as follows: assume $\frac{\mathrm{d}A}{\mathrm{d}t} = 0$ and then for $n = 1 : N$,

1. Use explicit Euler to update $C(nk)$ to $C((n+1)k)$. Note that in the case $\frac{\mathrm{d}C}{\mathrm{d}t} = rC$ for $r >> \gamma, \delta$ (i.e. in the case the system is stiff), an unconditionally stable backward difference method should be used.
2. Update $D((n+1)k)$ to satisfy (5.5)(a).
3. Use (5.5)(b) and the assumption that the ODEs (5.4) are at equilibrium to solve for $A((n+1)k))$ and $B((n+1)k)$.

Now, consider the proposed DAE method in which (5.5)(a) is used:

$$\begin{bmatrix} 1 & 0 & 0 & 0 \\ 0 & 1 & 0 & 0 \\ 0 & 0 & 1 & 0 \\ 0 & 0 & 0 & 0 \end{bmatrix} \begin{bmatrix} A'(t) \\ B'(t) \\ C'(t) \\ D'(t) \end{bmatrix} = \begin{bmatrix} -\gamma A + \delta BD \\ \gamma A - \delta BD \\ r \\ A + 2B - 2C - D \end{bmatrix}. \tag{5.6}$$

In the above system, D is the algebraic variable. Alternatively, we could make B the algebraic variable and use (5.5)(a)

$$\begin{bmatrix} 1 & 0 & 0 & 0 \\ 0 & 0 & 0 & 0 \\ 0 & 0 & 1 & 0 \\ 0 & 0 & 0 & 1 \end{bmatrix} \begin{bmatrix} A'(t) \\ B'(t)(t) \\ C'(t) \\ D'(t) \end{bmatrix} = \begin{bmatrix} -\gamma A + \delta BD \\ A + B - (A(0) + B(0)) \\ r \\ \gamma A - \delta BD \end{bmatrix}. \tag{5.7}$$

Expected behavior. Notice that there are two competing dynamics of the system: the disparity of the rate constants γ and δ and the conservation equations (5.5). Since $\delta >> \gamma$ by assumption, we expect D and B to approach zero while A grows rapidly. If this happens C must grow in order to satisfy (5.5)(a). However, C is not free to change its growth rate since r is fixed.

Since the DAE system (5.6) uses (5.5)(a), we expect that satisfying this condition will come at the cost of satisfying (5.5)(b). The opposite is expected of DAE system (5.7). Finally, we expect the solution obtained from the equilibrium method to satisfy both (5.5)(a) and (5.5)(b) since both are used in its solution.

Results. Let $T = 200$, $[A(0), B(0), C(0), D(0)]^T = [2, 1, 0, 4]^T$. Notice that (5.5)(a) is satisfied and that C will be supplied entirely through its linear source term. The rate constants are set as follows: $r = 0.01$, $\gamma = 1$, $\delta = 1 \times 10^4$. We examine the differences between small and large values of N, using $N = 10$ and $N = 1000$. Recall that `ode15s` is known to work well with stiff problems; since the ratio between our rate constants $\frac{\delta}{r}$ is large relative to our initial conditions, we will be using this solver.

In Figures 5.1a through 5.1f we notice that the results from the equilibrium method are indistinguishable from the results obtained from DAE (5.7), except for in Figure 5.1d where the ADE result has a steady value for D and the equilibrium method has D undergoing linear decay. To see the reason for this, consider Figure 5.1e where the quantity (5.5)(a) is shown. We see that the increase in (5.5)(a) mirrors the decay in D. From this figure, we infer that the reason for the decay is to satisfy (5.5)(a).

Recall that grid values of D are set to satisfy (5.5)(a) in the equilibrium assumption method. This allows the value of D to change whether or not its time derivative in (5.4) is nonzero. This results in nonphysical behavior since B should be changing at the same rate as D since their time derivatives are the same. We see the same issue

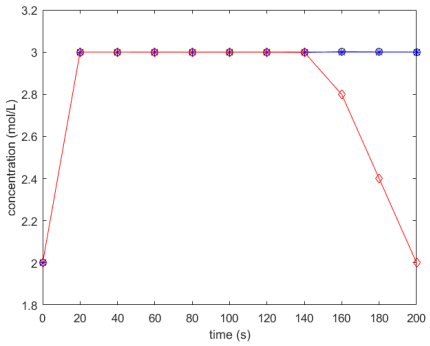

(a) Numerical solutions for A.

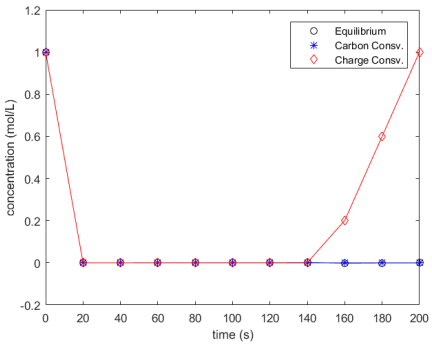

(b) Numerical solutions for B.

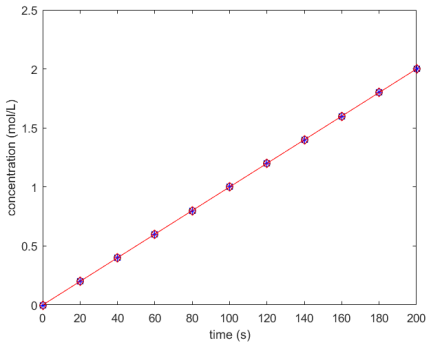

(c) Numerical solutions for C.

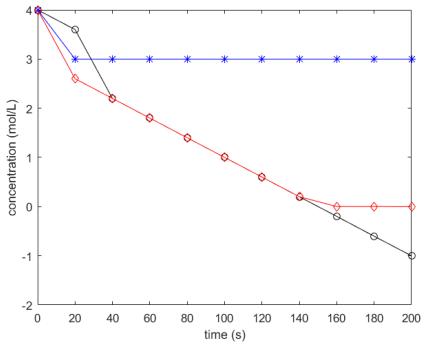

(d) Numerical solutions for D.

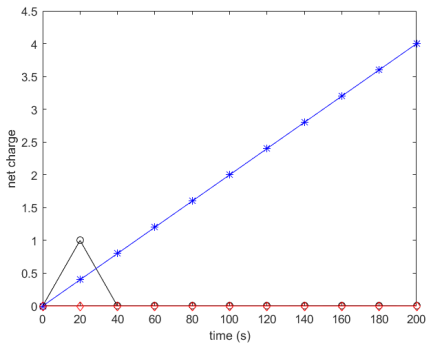

(e) $|A(t) + 2B(t) - 2C(t) - D(t)|$

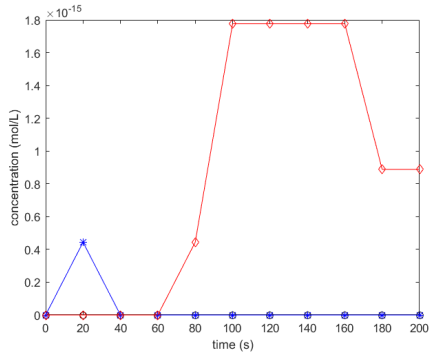

(f) $|A(t) + B(t) - (A(0) + B(0))|$

Figure 5.1: Numerical solutions of (5.4) with $N = 10$. The equilibrium and DAE (5.7) results agree while B becomes the favored product after $t = 140$ in DAE (5.6). All C results agree, which is not surprising given its simple linear source term. While D quickly reaches a steady state for DAE (5.7), it decreases for the other systems, taking on negative values for solution from the equilibrium assumption. The result from DAE (5.7) deviates significantly from (5.5)(a). No result deviates far from (5.5)(b), the largest value is $\approx 1.8 \times 10^{-15}$.

with the DAE (5.6) result; recall that DAE (5.6) was the algebraic system employing (5.5)(b). An important difference between these two results is that DAE (5.6) has no negative D values while the equilibrium solution does.

As expected, the solution obtained by applying DAE (5.7) satisfies (5.5)(b) at the expense of (5.5)(a). Meanwhile, DAE (5.6) satisfies both conservation equations. This is surprising since its formulation does not include (5.5)(b). However, after time $t = 140$ we observe that B increases at the same rate A decreases despite the rate disparity $\gamma << \delta$. Notice that this happens as D stops decreasing and that it causes $A+2B$ to become more positive We theorize the change in A's and B's growth patterns happens in order to satisfy (5.5)(a) since C is still increasing.

The results for the $N = 1000$ case are nearly the same as the $N = 10$ results. The graphs are sharper (which makes sense because the time step is much smaller), but the behavior of the solutions is the same.

5.3 Comparing ODE and DAE solutions of Robertson's problem

Consider the RREs that make up Robertson's problem, a well known test case that can be found in [1],

$$\begin{bmatrix} 1 & 0 & 0 \\ 0 & 1 & 0 \\ 0 & 0 & 1 \end{bmatrix} \begin{bmatrix} A'(t) \\ B'(t) \\ C'(t) \end{bmatrix} = \begin{bmatrix} -0.04A + 1 \times 10^4 BC \\ 0.04A - 1 \times 10^4 BC - 3 \times 10^7 B^2 \\ 3 \times 10^7 B^2 \end{bmatrix}, \qquad \begin{bmatrix} A(0) \\ B(0) \\ C(0) \end{bmatrix} = \begin{bmatrix} 1 \\ 0 \\ 0 \end{bmatrix}. \tag{5.8}$$

Numerical solvers may struggle to solve this stiff system since the extremely fast dynamics of the third reaction will require that the solution be calculated on a very fine grid. As previously mentioned, the native MATLAB solver `ode15s` is the recommended solver for stiff ODEs. This solver automatically refines the grid in order to satisfy a relative or absolute error tolerance that the user provides.

Notice that $A' + B' + C' = 0$; we can use this to show that the system satisfies a linear conservation law:

$$0 = \int_0^t (A'(t)+B'(t)+C'(t))\mathrm{d}t = A(t)+B(t)+C(t)-(A(0)+B(0)+C(0)) = A(t)+B(t)+C(t)-1.$$

As in Section 5.2, we can use the conservation law to formulate the problem as a DAE system:

$$\begin{bmatrix} 1 & 0 & 0 \\ 0 & 1 & 0 \\ 0 & 0 & 0 \end{bmatrix} \begin{bmatrix} A'(t) \\ B'(t) \\ C'(t) \end{bmatrix} = \begin{bmatrix} -0.04A + 1 \times 10^4 BC \\ 0.04A - 1 \times 10^4 BC - 3 \times 10^7 B^2 \\ 1 - A - B - C \end{bmatrix}, \qquad \begin{bmatrix} A(0) \\ B(0) \\ C(0) \end{bmatrix} = \begin{bmatrix} 1 \\ 0 \\ 0 \end{bmatrix}. \tag{5.9}$$

Recall that `ode15s` is also the recommended solver for stiff DAEs. Thus, we will use it to solve each system.

Solutions will be calculated from time $t = 0$ to $t = 10$ with discretization parameter $k = 2^{-n}$, $n = 11, \ldots, 15$. In lieu of an exact solution to Robertson's problem we calculate a fine grid solutions for each method using $k = 2^{-22}$. Let U_k^{ODE} and U_k^{DAE} refer to the solution vectors for the ODE and DAE method. Let $U_{\mathrm{fine}}^{\mathrm{ODE}}$ and $U_{\mathrm{fine}}^{\mathrm{DAE}}$ refer to vectors containing the fine grid solutions.

Note that the specific mesh sizes were chosen because the system dynamics are poorly captured for $n \leq 10$. Since the mesh corresponding to $n = 11$ is the coarsest reasonable mesh for this system, computation of the fine grid solution requires too much time to be feasible for this paper. For final times on the order of 10^2 or higher, the solution was too computational demanding to find. Numerical tests for larger

final times and coarser meshes were inconclusive because the coarser meshes failed to capture the stiff dynamics.

Results. We want to understand how the DAE and ODE solutions compare. To this aim, we plot the values

$$\|U_k^{\mathrm{ODE}} - U_{\mathrm{fine}}^{\mathrm{ODE}}\|_{\Delta,2},\ \|U_k^{\mathrm{DAE}} - U_{\mathrm{fine}}^{\mathrm{ODE}}\|_{\Delta,2},\ \|U_k^{\mathrm{ODE}} - U_{\mathrm{fine}}^{\mathrm{DAE}}\|_{\Delta,2},$$

and

$$\|U_k^{\mathrm{DAE}} - U_{\mathrm{fine}}^{\mathrm{DAE}}\|_{\Delta,2},$$

for each species A, B, and C and $k = 2^{-n}$, $n = 11, \ldots, 15$, in Figure 5.2. Figure 5.3 plots the same differences, but only their evaluation at the final time.

Figure 5.2: Plot of the values $\|U_k^{\mathrm{ODE}} - U_{\mathrm{fine}}^{\mathrm{ODE}}\|_{\Delta,2}$, $\|U_k^{\mathrm{DAE}} - U_{\mathrm{fine}}^{\mathrm{ODE}}\|_{\Delta,2}$, $\|U_k^{\mathrm{ODE}} - U_{\mathrm{fine}}^{\mathrm{DAE}}\|_{\Delta,2}$, and $\|U_k^{\mathrm{DAE}} - U_{\mathrm{fine}}^{\mathrm{DAE}}\|_{\Delta,2}$ for each species A, B, and C and $k = 2^{-n}$, $n = 11, \ldots, 15$. The various errors does not shed any light on convergence to the fine grid solutions. Note that the scale on the plot for Species A is quite different from the others due to its relatively small concentration.

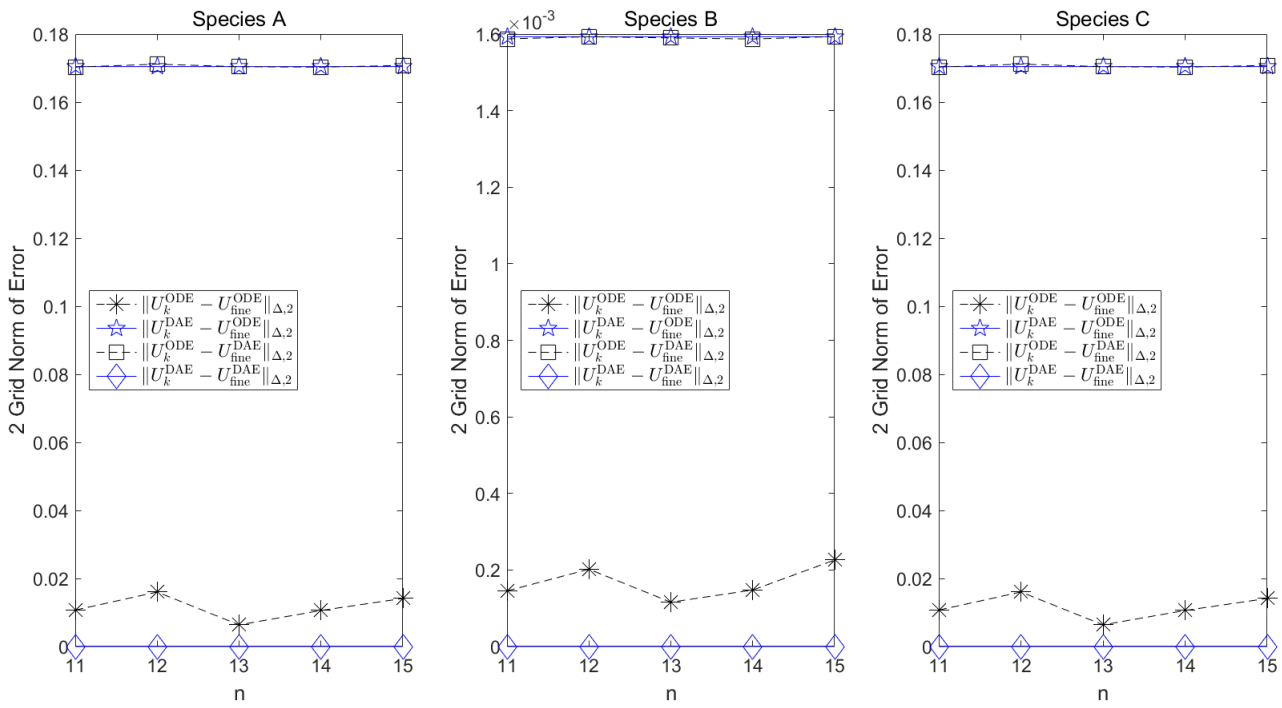

Now we discuss some of our findings. Note that since `ode15s` is a variable order method, it uses numerical differentiation formulas that are at least 1st order and at most 5th order. Thus, we expect to see at least 1st order convergence to the fine grid solution in the above figures. That the difference between the course DAE solutions and both the fine grid solutions remains relatively constant as we refine the grid is counter to our expectations. This is likely due to the fact that `ode15s` is a variable step method as well as a variable order method. While we provide it with a sequence of step sizes, those step sizes only influence the initial time step of the solver. As the solver moves forward, it is free to refine its step size.

Despite this, when we compare the cost of implementation of the two methods by solving the Robertson system as above 1×10^4 times for $k = 2^{-n}$, $n = 11, \ldots, 15$,

Figure 5.3: Plot of the errors at the end time $t = 10s$: $|U_k^{\text{ODE}} - U_{\text{fine}}^{\text{ODE}}|_{\text{end}}$, $|U_k^{\text{DAE}} - U_{\text{fine}}^{\text{ODE}}|_{\text{end}}$, $|U_k^{\text{ODE}} - U_{\text{fine}}^{\text{DAE}}|_{\text{end}}$, and $|U_k^{\text{DAE}} - U_{\text{fine}}^{\text{DAE}}|_{\text{end}}$ for each species A, B, and C and $k = 2^{-n}$, $n = 11, \ldots, 15$. These values do not shed any light on convergence to the fine grid solutions. Note that the scale on the plot for Species A is quite different from the others due to its relatively small concentration.

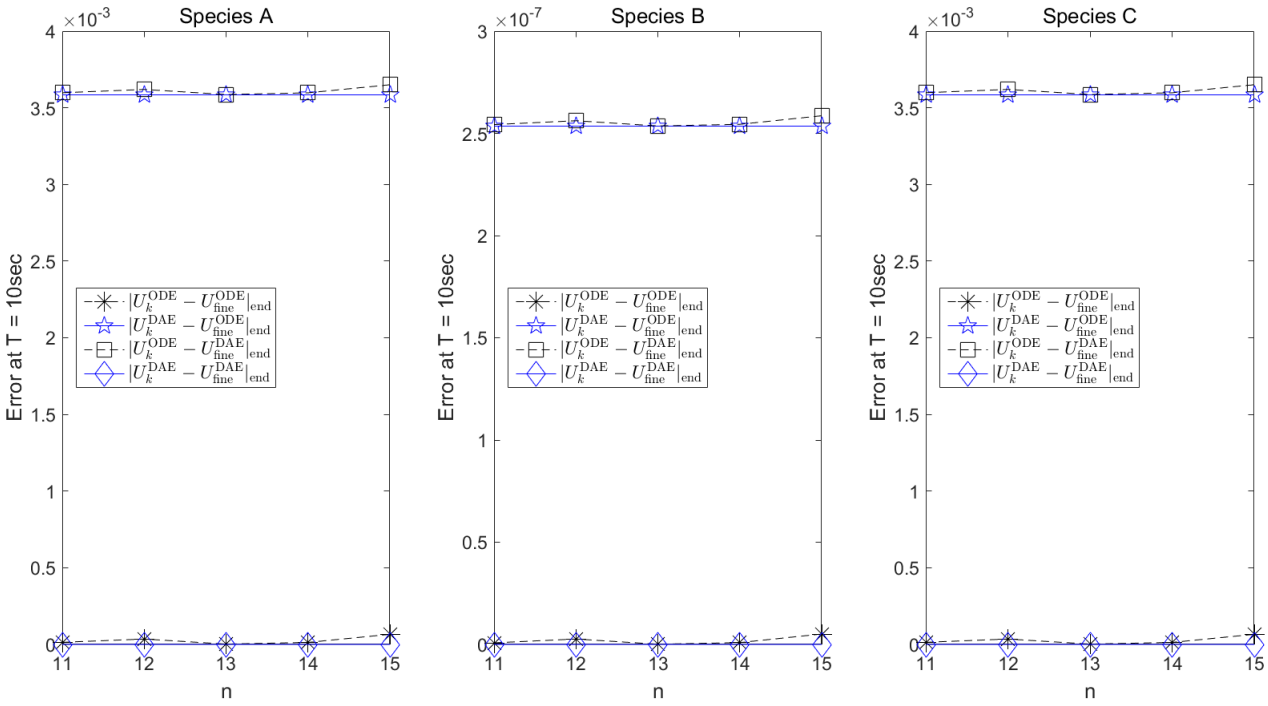

we find that computation time approximately doubles at each successive refinement. This indicates that the refinements do have an impact on `ode15s`'s treatment of the solution. Despite this, the numerical error does not improve. The computation times are included in Table 5.1; they do tell us that `ode15s` is more efficient at solving the ODE than the DAE but that the difference decreases as the provided time step is refined.

h	ODE ($s \times 10^4$)	DAE ($s \times 10^4$)	DAE/ODE (dimensionless)
2^{-11}	0.12498	0.13261	1.061
2^{-12}	0.23903	0.25195	1.054
2^{-13}	0.48395	0.48914	1.011
2^{-14}	0.95247	0.95812	1.006
2^{-15}	1.9331	1.9555	1.012

Table 5.1: Time to solve the ODE and DAE systems 10000 times for step sizes h.

Future tests. We identify three further tests the could help to compare the ODE and DAE formulations. First, one could do a tolerance refinement analysis using `ode15s` for the ODE and DAE formulations, and compare the rates of convergence for the two methods. Second, one could complete a fine grid comparison using a solver for which the user was in full control of the time steps. Third, one could model

a system which has slower moving dynamics. In this case, the numerical difficulties that the stiffness of Robertson's problem causes would not be conflated with the differences in the ODE and DAE formulations.

Chapter 6: Regularizing the discontinuous precipitation term

In this chapter, we consider the reaction rate equation (4.10) that arises at the precipitation stage of the calcite model. Since RRE (4.10) experiences a jump discontinuity when the reactant concentrations exceed a threshold value, its right hand size is not differentiable.

Recall from Section 2.1.3 that LTE analysis requires the ability to take Taylor series expansions of the solution about grid points. Thus, we have to be careful when analyzing the truncation error and the global error when solving (4.10). A potential way to solve this problem is to regularize the equation to make the right had size smooth for all t. Such an approach is common in mathematical analysis of ODEs and PDEs; we provide references to the MICP-related work below.

Notice that we can succinctly express (4.10) as

$$\frac{\mathrm{d}[\mathrm{CaCO_3}]}{\mathrm{d}t} = k_p(S-1)^2 H(S - S_{\mathrm{crit}}), \qquad H(x) = \begin{cases} 0 & \text{if } x < 0 \\ 1 & \text{if } x \geq 0. \end{cases} \tag{6.1}$$

In Section 6.1 we summarize the results of [5] in which the authors prove the well-posedness of a reactive transport model containing a discontinuous mineral precipitation reaction. One of the formulations they consider uses the Heaviside operator H. Next, in Section 6.2 we provide a brief background on Yosida approximations before considering their application to (6.1) in Section 6.3.

6.1 Well-posedness in reactive transport

In [5], the authors analyze the evolution of several aqueous chemical species with special focus on how to describe mineral precipitation-dissolution. There are three formulations of mineral reactions that they consider: set-valued rate function, complementary condition, and discontinuous rate function. While these are not pointwise equivalent, the authors are able to show that the formulations have the same weak solutions in $H^1(0,T)$ where $(0,T)$ is a finite time domain.

Next, they introduce a general reaction model in which the Heavyside formulation is used. Their boundary condition relies on a parameter β that can be selected to induce either homogenous Neumann conditions or a total normal flux that is equal to a given quantity. The model includes a finite number of species labeled as either "mobile" or "mineral," and a finite number of chemical reactions labeled as "kinetic" or "mineral." In showing the existence of a global solution to the general reaction model, they introduce a regularized version of the Heavyside function which linearly increases from 0 to 1 on an ϵ-neighborhood of the origin.

After introducing an a priori estimate, the authors are actually able to prove that there exists nonnegative (i.e. physically allowable) solutions to the model with the regularized Heavyside function. The main result, existence of nonnegative solutions to the model with the set-valued rate function, is shown to follow from this result by taking limits as ϵ approaches 0 from above.

This result is important because it preserves the physical interpretation of the system. This is in contrast to our results in Section 5.2 where the solver produced negative values in Figure 5.1d. The paper concludes with a proof of uniqueness in which the authors suppose there are two solutions to the general reaction model and then show they are equivalent.

6.2 Yosida approximations

For a given m-accretive operator A its Yosida approximation is a series of Lipschitz continuous operators A_α where $\alpha > 0$ is a parameter and $\lim_{\alpha\to 0} A_\alpha = A$ [14]. In particular, we can approximate graphs that have jump discontinuities or regions where the resulting graph is not a function. This is useful from the perspective of solving reaction rate equations such as (6.1) for which the reaction term is discontinuous. We can apply numerical methods to the Yosida approximations to obtain approximate solutions to the system. Recall that an operator A on $\mathbb{R}$ is accretive if $y_1 \in A(x_1)$, $y_2 \in A(x_2)$ implies that $(y_1 - y_2)(x_1 - x_2) \geq 0$. If A also has the property that the range of $I + A$ includes all of $\mathbb{R}$, then A is m-accretive.

In Section 6.2.1 we recall that definition of a Yosida approximation and give a visual examples of its application. We discuss its applications to ordinary differential equations in Section 6.2.3.

6.2.1 Constructing Yosida approximations

Consider an operator $A\colon \mathbb{R} \to \mathbb{R}$, and let I be the identity operator. To construct the Yosida approximation A_α we first need to construct the *resolvent* R_α. Let $\alpha \in \rho(A) = \{\alpha - IA \text{ is invertible}\}$, the resolvent set of A. Then

$$R_\alpha = (I + \alpha A)^{-1}. \tag{6.2}$$

Next, we use R_α to construct A_α:

$$A_\alpha = \frac{1}{\alpha}(I - R_\alpha). \tag{6.3}$$

In the following example, we consider the Yosida approximations of the operator $D = sgn^{-1}(x)$. We find that each D_α is Lipschitz continuous with constant $K = \frac{2}{\alpha}$.

6.2.2 Sign graph

The operator is $D = sgn^{-1}(x)$ has a graph of

$$sgn^{-1} = \{-1\} \times \{\mathbb{R}^-\} \cup (-1, 1) \times \{0\} \cup \{1\} \times \{\mathbb{R}^+\}.$$

Notice that $sgn^{-1}(v)$ is a multi-valued operator, and that it is not linear. However, we see that its Yosida approximation D_α is a single-valued linear operator for $\alpha > 0$:

$$D_\alpha = \left\{ \left(x, \frac{x+1}{\alpha} \right) : x < -1 \right\} \cup \{(x, 0) : x \in [-1, 1]\} \cup \left\{ \left(x, \frac{x-1}{\alpha} \right) : x > 1 \right\}.$$

Further, D_α is Lipschitz continuous with constant $\frac{2}{\alpha}$. To see this, fix two distinct real numbers x_1 and x_2 and consider the following cases:

(a) If $x_1 < -1$ and $x_2 < -1$, then

$$\frac{|D_\alpha(x_1) - D_\alpha(x_2)|}{|x_1 - x_2|} = \frac{|\alpha^{-1}(x_1 + 1) - \alpha^{-1}(x_2 + 1)|}{|x_1 - x_2|} = \frac{1}{\alpha}\frac{|x_1 - x_2|}{|x_1 - x_2|} = \frac{1}{\alpha}.$$

If $x_1 > 1$ and $x_2 > 1$, a similar result follows.

(b) If $x_1, x_2 \in [-1, 1]$, $D_\alpha(x_1) - D_\alpha(x_2) = 0$.

(c) If $x_1 < -1$ and $x_2 > 1$, then

$$\frac{|D_\alpha(x_1) - D_\alpha(x_2)|}{|x_1 - x_2|} = \frac{1}{\alpha}\frac{|x_1 - x_2 + 2|}{|x_1 - x_2|} \leq \frac{1}{\alpha}\left(1 + \frac{2}{|x_1 - x_2|}\right) < \frac{2}{\alpha},$$

where the last inequality is from the fact that $|x_1 - x_2| > 2$.

(d) If $x_1 < -1$ and $x_2 \in [-1, 1]$, then

$$\frac{|D_\alpha(x_1) - D_\alpha(x_2)|}{|x_1 - x_2|} \leq \frac{1}{\alpha}\frac{|x_1 + 1|}{|x_1 + 1|} = \frac{1}{\alpha}.$$

If $x_1 > 1$ and $x_2 \in [-1, 1]$, a similar result follows.

It is important to recognize that as $D_\alpha \to D$ and $\alpha \to 0$, the Lipschitz constant $\frac{2}{\alpha}$ blows up. We touch on this observation in Section 6.2.3.

Figure 6.1: The graph of $sgn^{-1}(x)$ is multi-valued while the Yosida approximation is single-valued. If we let α approach zero, the Yosida approximation will become increasingly steep as it approaches sgn^{-1}.

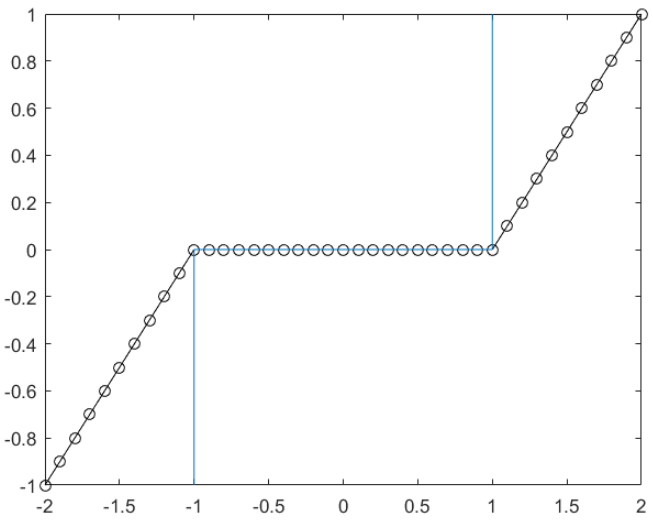

6.2.3 Application to ODEs

We begin by stating an existence and uniqueness theorem for ordinary differential equations, and then use this theory to inform our use of Yosida approximations. Consider the following initial value problem:

$$\begin{cases} \mathrm{d}v/\mathrm{d}t = f(t, v) \\ v(t_0) = a \end{cases} \tag{6.4}$$

An existence and uniqueness theorem from [4] is included below.

Theorem 1 *Let $f(t, v)$ be defined on a Banach space. Suppose f is bounded, Lipschitz continuous in v, and continuous at t_0. Then there exists a positive constant ϵ such that there is a unique solution to the above IVP on $[t_0 - \epsilon, t_0 + \epsilon]$.*

Consider the following initial value problem:

$$v' + Av(t) = 0, \quad v(t_0) = v_0. \tag{6.5}$$

If A is single-valued Lipschitz continuous operator, then we can use Theorem 1 to say that a unique solution exists on some neighborhood of t_0. Suppose A is a multivalued operator such as the Heavyside operator which satisfies the definition of being m-accretive. Instead of attempting to solve (6.5), we could pose a sequence of ODEs:

$$v' + A_\alpha v(t) = 0, \quad v(t_0) = v_0. \tag{6.6}$$

Since the Yosida approximation A_α is a Lipschitz function, the above Theorem guarantees us a unique solution to the IVP on some symmetric domain about t_0 for each choice of α. However, as we have seen in the example of the sgn^{-1} graph, the Lipschitz constant grows as α approaches zero. Therefore, we cannot necessarily compute a sequence of solutions v_α and assume $\lim_{\alpha\to 0} v_\alpha(x) = v(x)$ for all x in the domain of our problem.

We note that [13](Theorem 3.3, pg. 104) contains an existence and uniqueness theorem for which A is not restricted to being a Lipschitz continuous operator. A sufficient condition for a unique C^1 solution to the problem (assuming v_0 is in the domain of A) is that A be linear and that $-A$ be the generator of a contraction semigroup. However, the "A" that we will consider below is not linear.

6.3 Applying Yosida approximations to the calcite reaction

We will now apply a Yosida approximation to $H(S(t) - S_{\text{crit}})$ from RRE (6.1) to regularize its behavior about $S = S_{\text{crit}}$. The result will be an operator $H_\alpha(S(t) - S_{\text{crit}})$ which linearly increases from 0 to 1 on the interval $[0, \alpha]$. The effect is similar to the use of regularization in Chapter 3.

We present the regularized precipitation rate equation that results from this approximation in Equation 6.7 below.

$$R^\alpha(S(t)) = \begin{cases} 0, & \text{if } S(t) < S_{\text{crit}} \\ \frac{1}{\alpha}(S(t) - S_{\text{crit}}) \cdot (S(t) - 1)^2, & \text{if } S_{\text{crit}} \le S(t) < S_{\text{crit}} + \alpha \\ (S(t) - 1)^2, & \text{if } S(t) \ge S_{\text{crit}} + \alpha. \end{cases} \tag{6.7}$$

Notice that Equation 6.7 agrees with Equation 6.1 when $S(t) < S_{\text{crit}}$ and when $S(t) \ge S_{\text{crit}} + \alpha$. The domain on which they disagree, $S_{\text{crit}} \le S(t) < S_{\text{crit}} + \alpha$, is controlled by our choice of α.

We note that smoothing the calcite precipitation rate equation has a physical interpretation. In reality, chemical reactions do not operate on a "100% on, 100% off" basis as in (6.1). In contrast, the rate of the phase transition from aqueous Ca^{2+} and CO_3^{2-} ions to solid $CaCO_3$ will likely increase from extremely small for $S < S_{\text{crit}}$ to $k_p(S-1)^2$ for $S > S_{\text{crit}}$ on some neighborhood of S_{crit}. We think of the this neighborhood as coinciding with the neighborhood on which we smooth the rate equation.

Now we show some solutions to the problem with the regularized reaction rate. We obtain these solutions using the explicit Euler finite difference approximation. Figure 6.2 below compares solutions to Equation (6.1) and (6.7) assuming that the calcium and carbonate ions have source rates of 0.2mol/s and 0.1mol/s, respectively. We set $S_{\text{crit}} = 2$ and use $\alpha = 0.5$. The solution to (6.7) appears smoother than the solution to (6.1). Additionally, the solutions seem to agree in regards to the long-term behavior of solutions. Further analysis is needed to confirm the usefulness of this regularization.

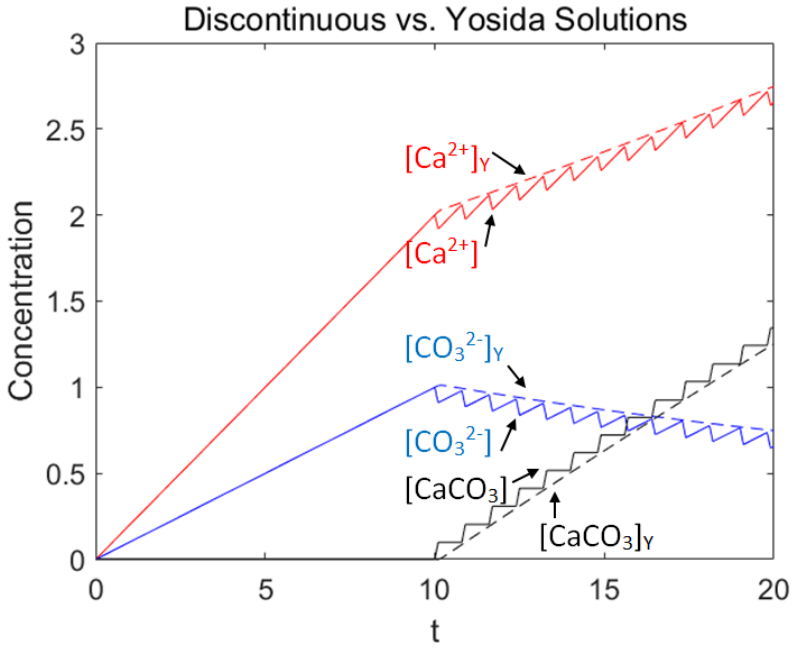

Figure 6.2: The solutions obtained after applying the Yosida approximation $[\,\cdot\,]_Y$ are smoother than the solutions from the discontinuous reaction $[\,\cdot\,]$. The solutions for each species follow the same trend as their concentrations increase.

Chapter 7: Coupled Advection-Diffusion-Reaction System

In this chapter we will use the fractional step method from Section 2.3 to solve a coupled advection-diffusion-reaction system. The species and reactions involved are the same as those discussed in Section 5.1:

$$[CO_3^{2-}] + 2[OH^-] \underset{B_1}{\overset{F_1}{\rightleftharpoons}} [HCO_3^-] + [OH^-] \underset{B_2}{\overset{F_2}{\rightleftharpoons}} [CO_3^{2-}], \qquad [NH_3] \underset{B_3}{\overset{F_3}{\rightleftharpoons}} [NH_4^+] + [OH^-].$$

However, instead of using the rate constants from [17] which take the form $\frac{F_i}{B_i} = K_i$ and are on the order 1×10^1, we will be prescribing rate constants on the order of 1×10^0. The slower moving dynamics will make it easier to tell if the fractional step method is working correctly.

After prescribing homogeneous boundary conditions we see that our problem is to solve seven coupled two-point boundary problems of the form

$$(u_i)_t + a(u_i)_x - d(u_i)_{xx} = r_i(u), \qquad \begin{array}{l} x \in (0,1), \quad 0 < t \leq 25, \\ u_i(0,t) = 0, \quad (u_i)_x(1,t) = 0, \\ u_i(x,0) = f_i(x), \end{array}$$

where each u_i, $1 \leq i \leq 7$, is a different chemical species. These problems are coupled through the reaction terms, $r_i(u)$. Unless otherwise stated, $a = 9.5 \times 10^{-3}$ and $d = 1 \times 10^{-4}$. We choose a to be approximately two orders of magnitude larger than d so that transport dominates the smoothing effect of diffusion. That is, we seek to preserve the profiles of the chemical species as the system is solved so that the reaction dynamics are more easily observed.

For the numerical solution, we set the following discretization. The spatial mesh size is $h = 1 \times 10^{-4}$ and in time we use $k = 1 \times 10^{-2}$. Note that these values satisfy $|\frac{ak}{h}| < 1$; the upwind method as discussed in Section 2.1.1 is stable.

In Section 7.1 we test whether or not Newton's method produces results in line with physical expectations. To do this, we will set the initial conditions $f_i(x)$ so that the reactants are isolated. This will allow us to If the method works as expected on this test case, no reactions will take place until advection brings the reactants in contact with one another.

In Section 7.2 we test whether or not it is necessary to include the carbon and nitrogen conservation laws discussed in Section 4.4. Thus, we will use no flux boundary conditions $(u_i)_x(0,t) = (u_i)_x(1,t) = 0$ to ensure minimal amounts of the species leave the system. In order to simplify the dynamics, we will assume that each species has the same initial profile. If the total amount of carbon and nitrogen in the system changes as the solution evolves for this simple test case, it will support the inclusion of the conservation laws.

7.1 Isolated initial conditions

Consider the following initial concentration profiles:

$$[NH_3](x,0) = [H_2CO_3](x,0) = \begin{cases} 1, & \text{if } 0.1 \le x \le 0.25 \\ 0, & \text{otherwise} \end{cases}$$

$$[OH^-](x,0) = \begin{cases} 1, & \text{if } 0.4 \le x \le 0.55 \\ 0, & \text{otherwise} \end{cases}$$

$$[NH_4^+](x,0) = [HCO_3^-](x,0) = [CO_3^{2-}](x,0) = [H^+](x,0) = 0.$$

Notice that none of the reactions should occur at $t = 0$ since none of the reactants have nonzero concentrations in the same place. As the solution evolves, the positive advection constant will move the initial profiles to the right. Once $[NH_3]$ and $[OH^-]$ have nonzero, overlapping concentrations, we expect for $[NH_4^+]$ to form. Similarly, we expect $[HCO_3^-]$ to form once $[H_2CO_3]$ and $[OH^-]$ overlap.

We will set $F_1 >> B_1$ and $F_3 << B_3$ so that the $[H_2CO_3]$ and $[HCO_3^-]$ are the favored products in their respective reactions:

$$\begin{array}{c|c|c} F_1 = 3 & F_2 = 0.1 & F_3 = 0.1 \\ B_1 = 0.1 & B_2 = 0 & B_3 = 3 \end{array}$$

Additionally, we will set the advective constant for $[OH^-]$ equal to zero so that its concentration is stationary. This will ensure that the products are formed on a localized region, allowing us to see their final concentrations more clearly. The final profiles of our species of interest are plotted next to their initial profiles in Figure 7.1 below.

Figure 7.1: Final and initial profiles for $[NH_3]$, $[H_2CO_3]$, $[NH_4^+]$, $[OH^-]$, and $[HCO_3^-]$. Notice that the formation of the products $[NH_4^+]$ and $[HCO_3^-]$ is localized to the region where the curves for $[NH_3]$ and $[H_2CO_3]$ meet $[OH^-]$, respectively. Markers are included at every 1000'th grid point.

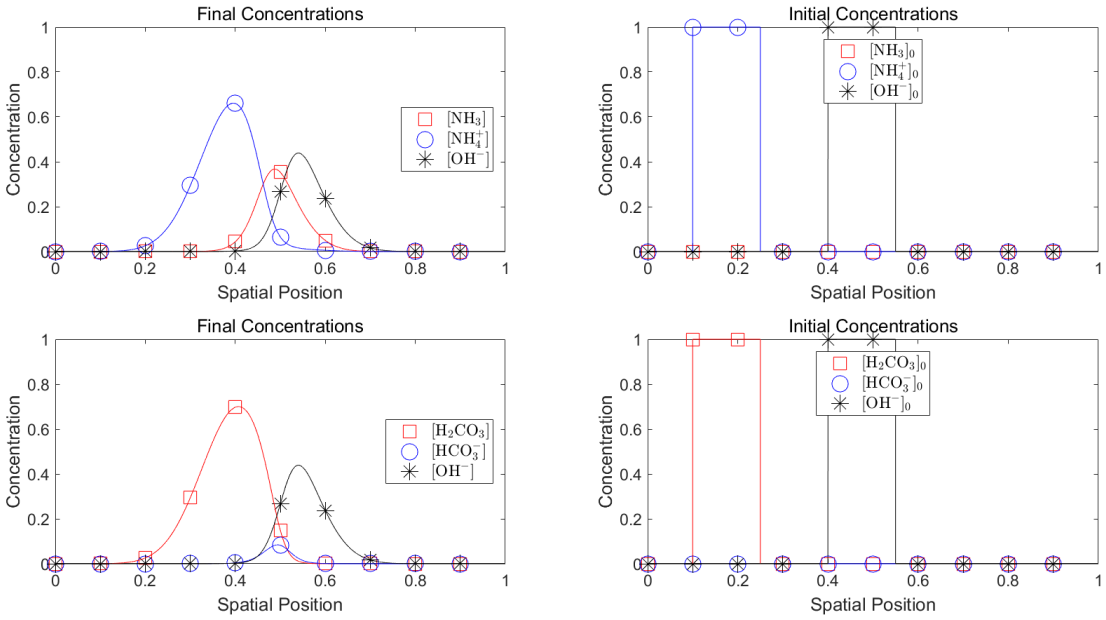

The results are as expected. The formation of the products $[NH_4^+]$ and $[HCO_3^-]$ is localized to the region where the curves for $[NH_3]$ and $[H_2CO_3]$ meet $[OH^-]$, respectively.

7.2 Results without using conservation laws

To keep track of the total amount of carbon and nitrogen in the system we use the approximations

$$\begin{aligned} C(t) &= \sum_{i=0}^{1\times 10^4-1} \left([\mathrm{H_2CO_3}](ih,t) + [\mathrm{HCO_3^-}](ih,t) + [\mathrm{CO_3^{2-}}](ih,t)\right)\cdot h \\ &\approx \int_0^1 \left([\mathrm{H_2CO_3}](x,t) + [\mathrm{HCO_3^-}](x,t) + [\mathrm{CO_3^{2-}}](x,t)\right)\mathrm{d}x \end{aligned}$$

and

$$\begin{aligned} N(t) &= \sum_{i=0}^{1\times 10^4-1} \left([\mathrm{NH_3}](ih,t) + [\mathrm{NH_4^+}](ih,t)\right)\cdot h \\ &\approx \int_0^1 \left([\mathrm{NH_3}](x,t) + [\mathrm{NH_4^+}](x,t)\right)\mathrm{d}x. \end{aligned}$$

We will keep track of these values on a relatively simple test case. If the carbon and nitrogen levels are not preserved, it is unlikely that they would be preserved on a system with faster dynamics.

We will use the same initial profile for each species:

$$[\cdot](x,0) = \begin{cases} x, & \text{if } 0 \le x \le 0.5 \\ 1, & \text{if } 0.5 \le x \le 1. \end{cases}$$

We will set the rate constants so that the maximum ratio of one to another is 3 to ensure that the system is not stiff:

$$\begin{array}{c|c|c} F_1 = 3 & F_2 = 1 & F_3 = 1 \\ B_1 = 2 & B_2 = 2 & B_3 = 2 \end{array}$$

Figure 7.2 below contains a plot of $C(t)$ and $N(t)$ for $0 \le t \le 25$.

We see that while the amount of carbon in the system stays constant as time progress, the amount of nitrogen increases steeply from $N(0) = 2$ to $N(2) \approx 2.3$ before leveling off for the remainder of the solution. This is despite the fact that no-flux boundary conditions were prescribed. We conclude that it may be necessary to use chemical conservation laws in the process of solving the system as in Section 4.4.

Figure 7.2: We plot $C(t) \approx \int_0^1 \left([\mathrm{H_2CO_3}](x,t) + [\mathrm{HCO_3^-}](x,t) + [\mathrm{CO_3^{2-}}](x,t)\right) \mathrm{d}x$ and $N(t) \approx \int_0^1 \left([\mathrm{NH_3}](x,t) + [\mathrm{NH_4^+}](x,t)\right) \mathrm{d}x$ for $0 \leq t \leq 25$. We see that the amount of carbon and nitrogen in the system (as measured by $C(t)$ and $N(t)$, respectively) is not constant. Markers are included every 500'th time step.

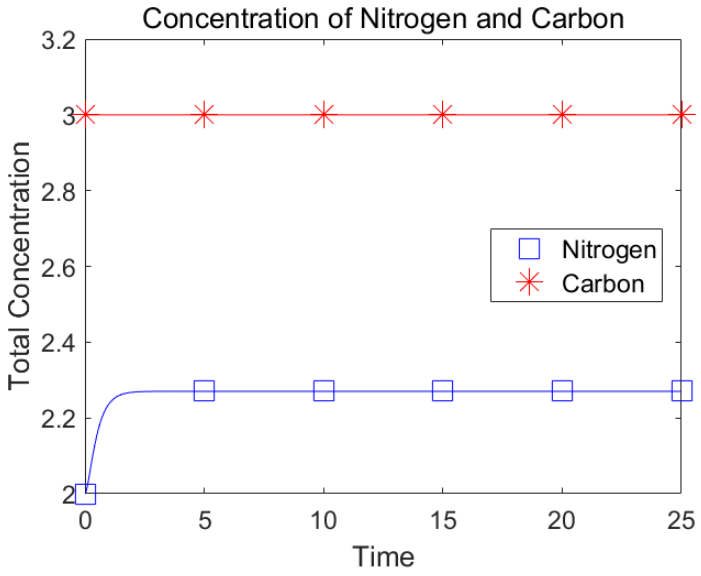

Chapter 8: Conclusions

In this paper we introduced numerical methods for the solution of systems of chemical reactions in the form of finite differences and nonlinear root finding techniques. We used these to test proposed modifications to a numerical solution solution scheme for a model of calcite precipitation, which has important applications.

The main motivation was to show that there are multiple directions from which one can approach the solution of a system of chemical reactions, and that there are multiple sensitivities to every element of this very complex system. Varying the treatment of any one of these elements can change its solution, and can propagate to different parts of the system.

In particular, we found that describing a system of reactions as a system of differential algebraic equations by including a conservation law produced different results than if that system had been solved as a system of ordinary differential equations. When testing to see if the two different formulations converged to different fine grid solutions, we discovered that the MATLAB solver `ode15s` did not allow us to control the step sizes used in the solution of the problem. Instead, the user controls the tolerances used in the calculation of the solution. We did find that the solution of the ODE formulation consistently took longer to find than the solution of the DAE formulation, but this difference decreased as finer grids were used.

Next, the discontinuous calcite reaction was regularized in an attempt to improve the numerical accuracy of the solution. We explained how this regularization could be viewed as an application of Yosida approximations. We found that the solution to the regularized reaction was linear while the solution to the discontinuous reaction was continuous but only piecewise linear.

Finally, we incorporated advection and diffusion terms into the reaction rate model and posed a two point boundary value problem with zero flux conditions to test whether or not it is necessary to include atomic conservation laws when solving a chemical system. The results showed that without the conservation law, elements did not remain in the system in the same quantities throughout the duration of the solution.

Future work in this area is to compare the effects of the above modifications on the solution to the entire calcite precipitation reaction model. One would need to determine some way to obtain a "true" solution to the model in order to test whether or not the proposed modifications are significant in reducing the numerical error.

Bibliography

[1] U. M. Ascher and L. R. Petzold, *Computer methods for ordinary differential equations and differential-algebraic equations*, Society for Industrial and Applied Mathematics (SIAM), Philadelphia, PA, 1998.

[2] E. Godlewski and P.-A. Raviart, *Numerical approximation of hyperbolic systems of conservation laws*, vol. 118 of Applied Mathematical Sciences, Springer-Verlag, New York, 1996.

[3] D. J. Higham, *Modeling and simulating chemical reactions*, SIAM Rev., 50 (2008), pp. 347–368.

[4] M. W. Hirsch, S. Smale, and R. L. Devaney, *Differential equations, dynamical systems, and an introduction to chaos*, Elsevier/Academic Press, Amsterdam, third ed., 2013.

[5] J. Hoffmann, S. Kräutle, and P. Knabner, *Existence and uniqueness of a global solution for reactive transport with mineral precipitation-dissolution and aquatic reactions in porous media*, SIAM J. Math. Anal., 49 (2017), pp. 4812–4837.

[6] J. Hommel, E. Lauchnor, A. Phillips, R. Gerlach, A. B. Cunningham, R. Helmig, A. Ebigbo, and H. Class, *A revised model for microbially induced calcite precipitation: Improvements and new insights based on recent experiments*, Water Resour. Res., 51 (2015).

[7] C. T. Kelley, *Iterative methods for linear and nonlinear equations*, vol. 16 of Frontiers in Applied Mathematics, Society for Industrial and Applied Mathematics (SIAM), Philadelphia, PA, 1995.

[8] J. D. Lambert, *Computational methods in ordinary differential equations*, John Wiley & Sons, London-New York-Sydney, 1973.

[9] A. C. Lasaga, *Kinetic theory in the earth sciences*, Princeton University Press, Princeton, NJ, 2014.

[10] R. J. LeVeque, *Finite difference methods for ordinary and partial differential equations*, Society for Industrial and Applied Mathematics (SIAM), Philadelphia, PA, 2007.

[11] R. H. Petrucci and W. S. Harwood, *General chemistry, principles and modern applications*, J. Chem. Educ., 74 (1997), p. 491.

[12] M. Shearer and R. Levy, *Partial differential equations*, Princeton University Press, Princeton, NJ, 2015.

[13] R. E. Showalter, *Hilbert space methods for partial differential equations*, Pitman, London-San Francisco, Calif.-Melbourne, 1977.

[14] ——, *Monotone operators in Banach space and nonlinear partial differential equations*, vol. 49 of Mathematical Surveys and Monographs, American Mathematical Society, Providence, RI, 1997.

[15] T. Zhang, N. G. Cogan, and Q. Wang, *Phase field models for biofilms. I. Theory and one-dimensional simulations*, SIAM J. Appl. Math., 69 (2008), pp. 641–669.

[16] ——, *Phase field models for biofilms. II. 2-d numerical simulations of biofilm-flow interaction*, Commun. Comput. Phys., 4 (2008), pp. 72–101.

[17] T. Zhang and I. Klapper, *Mathematical model of biofilm induced calcite precipitation*, WST, 61 (2010), pp. 2957–64.